Meereswissenschaftliche Berichte

Marine Science Reports

No. 87 2012

A regional 3D coupled ecosystem model of the Benguela upwelling system

Martin Schmidt, Anja Eggert

"Meereswissenschaftliche Berichte" veröffentlichen Monographien und Ergebnisberichte von Mitarbeitern des Leibniz-Instituts für Ostseeforschung Warnemünde und ihren Kooperationspartnern. Die Hefte erscheinen in unregelmäßiger Folge und in fortlaufender Nummerierung. Für den Inhalt sind allein die Autoren verantwortlich.

"Marine Science Reports" publishes monographs and data reports written by scientists of the Leibniz Baltic Sea Research Institute Warnemünde and their co-workers. Volumes are published at irregular intervals and numbered consecutively. The content is entirely in the responsibility of the authors.

Schriftleitung: Dr. Norbert Wasmund
(norbert.wasmund@io-warnemuende.de)

Bezugsadresse/address for orders:

Leibniz-Institut für Ostseeforschung Warnemünde
Bibliothek
Seestr. 15
18119 Rostock-Warnemünde
Germany
(bibliothek@io-warnemuende.de)

Eine elektronische Version ist verfügbar unter / An electronic version is available on:
http://www.io-warnemuende.de/marine-science-reports.html

The reports should be cited: Meereswiss. Ber., Warnemünde

ISSN 0939 -396X

Meereswissenschaftliche Berichte
MARINE SCIENCE REPORTS

No. 87

A regional 3D coupled ecosystem model of the Benguela upwelling system

by
Martin Schmidt, Anja Eggert

Leibniz-Institut für Ostseeforschung
Warnemünde
2012

Contents

Abstract

A regional 3-dimensional ecosystem model is presented designed to simulate the nutrient and oxygen dynamics in the Benguela upwelling system. Strong upwelling driven by the southern trade winds supply cold, nutrient rich water. This supports a high primary production and results in a large flux of sinking detritus. Hence, a thick organic-rich mud belt is characteristic for the Namibian continental shelf. Both biological and hydrodynamic processes contribute to the very specific geochemistry on the Namibian shelf. Notably high rates of sulfate reduction in the sediment generate high concentrations of dissolved hydrogen sulfide in the surface sediment layers and may be released intermittently to the water column. Large chemoautotrophic sulfur bacteria thrive on hydrogen sulfide and form conspicuous mats on the sediment. Denitrification and nitrification are important components of the nitrogen cycle and anaerobic ammonium oxidation is known to play a significant role as a nitrogen sink in the Benguela upwelling system. Organisms at higher trophic levels like zooplankton play an important role for mineralisation but also for the vertical and lateral transport of organic matter. The physical model component is *MOM-4* (Geophysical Fluid Dynamics Laboratory, GFDL). The ecosystem model is a NPZD-model (Nutrients-Phytoplankton-Zooplankton-Detritus) and is an extension of the ecosystem model ERGOM (Fennel & Neumann, 2004). Three phytoplankton and three zooplankton functional types are distinguished. All ecologically relevant processes mediated by prokaryotes in this ecosystem are implemented and the environmental conditions (e.g. oxygen concentration, temperature etc.) define the metabolic rates. The regional ecosystem model is tailored to the specific oxygen and sulfur dynamics on the shelf and simulates both processes in the water column and in the sediment. This model has been developed within the GENUS-project (Geochemistry and Ecology of the Namibian Upwelling System) funded by the German Federal Ministry of Education and Research (BMBF, reference number 03F0497A). It is an endorsed project of the Integrated Marine Biogeochemistry and Ecosystem Research (IMBER).

Kurzfassung

Es wurde ein regionales 3-dimensionales Ökosystemmodell entwickelt, dass die Nährstoff- und Sauerstoffdynamiken im Benguela Auftriebsgebiet simuliert. Angetrieben durch den Südost-Passat wird kaltes, nährstoffreiches Wasser in die Deckschicht aufgetrieben. Das wiederum ist die Grundlage einer hohen Primärproduktion und totes organisches Material sinkt in hohen Raten in die Bodenschicht ab. Ein biomassereicher Schlammgürtel kennzeichnet die Schelfregion vor Namibia. Sowohl biologische als auch hydrodynamische Prozesse bewirken die sehr spezifischen geochmischen Sedimenteigenschaften auf dem Namibischen Schelf. Insbesondere hohe Sulfatreduktionsraten in den Sedimenten produzieren hohe Schwefelwasserstoffkonzentrationen in den oberen Sedimentschichten und Schwefelwasserstoff kann auch sporadisch in die Wassersäule austreten. Große chemoautotrophe Schwefelbakterien leben von der Oxidation des Schwefelwasserstoffs und bilden auffällige Bakterienmatten auf der Sedimentoberfläche. Denitrifizierung und Nitrifizierung sind wichtige Komponenten des Stickstoffzyklus und Anaerobe Ammoniumoxidation ist eine signifikante Stickstoffsenke im Benguela Auftriebsgebiet. Organismen auf höheren trophischen Ebenen wie das Zooplankton spielen sowohl eine wichtige Rolle in der Mineralisierung als auch im vertikalen und lateralen Transport von organischem Material. Die physikalische Modellkomponente ist *MOM-4* (Geophysical Fluid Dynamics Laboratory, GFDL). Das Ökosystemmodell ist ein NPZD-Modell (Nährstoffe-Phytoplankton-Zooplankton-Detritus) und ist eine Weiterentwicklung des Ökosystemmodells ERGOM (Fennel & Neumann, 2004). Je drei funktionelle Gruppen werden für das Phytoplankton und das Zooplankton unterschieden. Alle ökologisch relevanten mikrobiellen Prozesse im Ökosystem sind implementiert und die Umweltbedingungen (z.B. Sauerstoffkonzentration, Temperatur) bestimmen die Umsatzraten. Das regionale Ökosystemmodell ist auf die speziellen Sauerstoff- und Schwefeldynamiken auf dem Schelf zugeschnitten und simuliert sowohl die Prozesse in der Wassersäule als auch im Sediment. Das Modell wurde im Rahmen des Projektes GENUS (Geochemistry and Ecology of the Namibian Upwelling System) entwickelt und ist finanziert vom Bundesministerium für Bildung und Forschung (BMBF, Förderkennzeichen 03F0497A). Das Projekt ist Teil des internationalen Forschungsverbundes IMBER (Integrated Marine Biogeochemistry and Ecosystem Research).

1 Introduction

The Benguela upwelling system along the south-western African continental margin is part of the eastern boundary current system of the South Atlantic Ocean. It sustains some of the highest rates of primary production in the ocean world-wide (Chapman & Shannon, 1985), which in turn feeds organisms on the higher trophic levels including high pelagic fish abundance. A developed fishing industry in Namibia and South Africa substantially changed the ecosystem since preindustrial time (Watermeyer et al., 2008a,b). However, large fluctuations were also observed of many other ecosystem variables.

The dynamics of the Benguela upwelling system is influenced by both, local winds and radiative forcing as well as remotely by coastal currents as the Angola or the Benguela current which propagate matter and momentum over large distances. Namely the Angola current, which can be considered as continuation of the equatorial current system bending southward at the African coast, carries pole-ward nutrient rich but oxygen-depleted water. The relatively cold water of the Benguela upwelling zone is bounded to the north by a frontal zone with a rapid transition to warm surface waters, the so called Angola-Benguela frontal zone.

The focus of the regional model is on the Benguela upwelling area and the Angola-Benguela frontal zone, which is part of the Benguela Current Large Marine Ecosystem (Fig. 1.1). The model area, however, is extended and also covers the southern trade wind zone and the equatorial currents. This is an appropriate choice, because the prescription of reasonable boundary values for the biochemical properties of Angola current waters propagating southward appeared difficult. Hence, the equatorial current system has been included into the model domain to have enough distance between the model boundaries and the area of interest. The western boundary of the model area is at 10°W and the southern boundary is approximately the latitude of Cape Town. Here open boundary conditions (OBC) apply. The model area is limited to the north and to the east by the African continent.

Although the upwelling water is generally well oxygenated ($[O_2] > 200\,\mu M$), low oxygen events within the Benguela upwelling system are well known (Chapman & Shannon, 1985). Hypoxic events ($[O_2] < 60\,\mu M$) within the northern and southern Benguela regions have somewhat different origins. In the northern part, they are caused by upwelling of low oxygen water originating from the Angola Basin. These events have a decadal time scale (Boyd et al., 1987). In the southern part, however, oxygen-depletion is primarily caused by high mineralisation rates of microorganisms. Especially expansive diatom blooms but also red-tides dominated by dinoflagellates in the euphotic layer (Pitcher et al., 1998) are displaced offshore with the surface Ekman transport. This results in a large flux of sinking detritus below the Ekman layer and advection back onto the shelf with the onshore Ekman compensation current. As a result, a thick organic-rich (diatomaceous) mud belt is characteristic for the ecosystem on the Namibian continental shelf. The consumption of oxygen during aerobic mineralisation of plankton biomass results in severely oxygen-depleted ($[O_2] < 10\,\mu M$) near bottom waters over large areas of the southwest African shelf. Physical processes which may transport oxygen from the euphotic zone to the deeper ocean or the sediment are usually weak. This contribute to the very specific sediment geochemistry of the Benguela continental shelf sediments. Notably high rates of sulfate reduction generates high concentrations of dissolved hydrogen sulfide (H_2S)

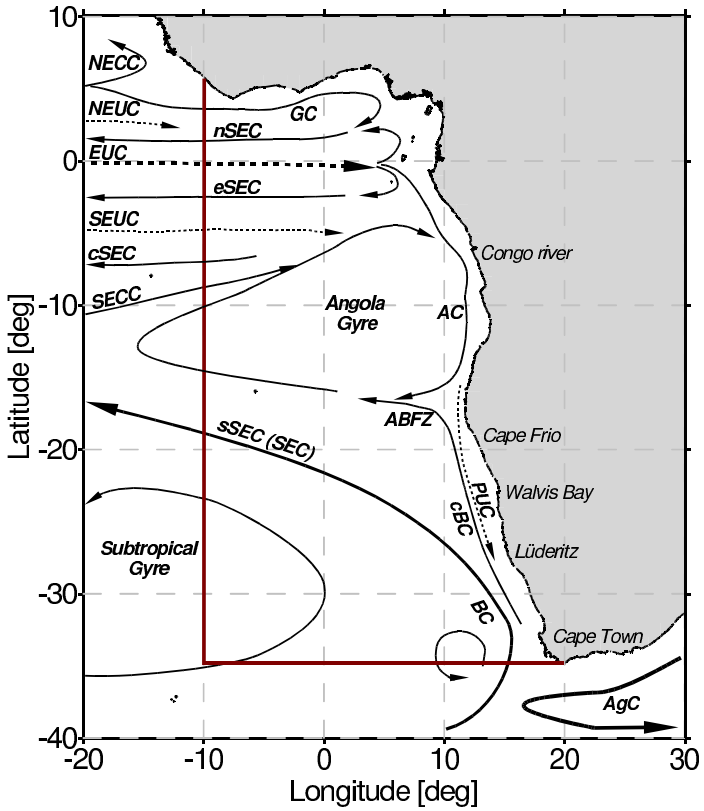

Fig. 1.1
Sketch of important horizontal near-surface ciruclations (full line) and circulations in the thermocline (dashed line) in the Benguela Current Large Marine Ecosystem. The red lines mark the model domain where open boundary conditions apply. Shown are the North Equatorial Counter Current (NECC), the North Equatorial Undercurrent (NEUC), the Guinea Current (GC), the northern (nSEC), equatorial (eSEC), central (cSEC), southern South Equatorial Current(sSEC), the Equatorial Undercurrent (EUC), South Equatorial Undercurrent(SEUC), the South Equatorial Contercurrent (SECC), the Angola Current (AC), the Angola Benguela Frontal Zone (ABFZ), the coastal (cBC) and the Benguela Current (BC), the Polar Undercurrrent (PUC), and the Agulhas Current (AgC) (adopted from Lass & Mohrholz (2008)).

Abb. 1.1
Skizze der wichtigsten horizontalen Oberflächenströme (durchgezogene Linien) und Ströme in der Thermokline (gestrichelte Linien) im Benguela-Ökosystem. Die rote Linie kennzeichnet das Modellgebiet an denen offene Randbedingungen vorliegen. Dargestellt sind der Nordäquatoriale Gegenstrom (NECC), der Nordäquatoriale Unterstrom (NEUC), der Guineastrom (GC), der nördliche (nSEC), äquatoriale (eSEC), zentrale (cSEC), südliche Südäquatoriale Strom (sSEC), der Äquatoriale Unterstrom (EUC), der Südäquatoriale Unterstrom (SEUC), der Südäquatoriale Gegenstrom (SECC), der Angolastrom (AC), die Angola-Benguela Front (ABFZ), der Küsten- (cBC) und der Benguelastrom (BC), der Polare Unterstrom (PUC), und der Agulhasstrom (AgC) (angepasst aus Lass & Mohrholz (2008)).

which can accumulate in the surface sediment layers and may even be released to the water column by means of episodic gas eruptions (DUNKER, 2005).

A 3-dimensional ecosystem model has been developed which is explicitly adapted to the Benguela upwelling system. The physical model part appropriately describes those processes, which govern the water mass properties on the shelf. Upwelled water is mainly a mixture of South Atlantic Central Water (SACW) and Eastern South Atlantic Central Water (ESACW), which have similar temperature and salinity characteristics but differ substantially in oxygen and nutrient concentration (LASS & MOHRHOLZ, 2005; MOHRHOLZ ET AL., 2008). The model area covers those regions, which govern the transport of ESACW and SACW onto the Namibian shelf. To account for the local modification of the biogeochemical water mass properties (MONTEIRO ET AL., 2006), a regional ecosystem model is employed, which is tailored for the specific oxygen and sulfur dynamics on the shelf. The model also includes nutrient cycling in the sediments and distinguishes between thin oxic and thick anoxic sediments, the latter beeing covered by thick mats of large sulfur bacteria. The physical model component is derived from *MOM-4* (GRIFFIES, 2009) (version *MOM-4*) and the description is restricted to additionally implemented features and major code modifications. The ecosystem model is plugged directly into the tracer scheme. It is an extension of the ecosystem model *ERGOM* (FENNEL & NEUMANN, 2004). With respect to the biogeochemical model part, it is a NPZD-model (Nutrients-Phytoplankton-Zooplankton-Detritus). Phytoplankton and zooplankton are the two biotic components and higher trophic levels (e.g. fish) are only implicitly part of the zooplankton mortality. Bacteria are not explicitly modeled, but are assumed to be omnipresent in the ecosystem. All ecologically relevant processes mediated by prokaryotes are implemented and solely the environmental conditions (e.g. oxygen concentration, temperature etc.) define the metabolic rates.

This technical report describes the relevant biogeochemical and metabolic processes in the Benguela upwelling system and summarizes the basic equations of both the ecosystem and the physical model components.

2 The 3D biogeochemical ecosystem model

2.1 State variables and processes

A Nutrient-Phytoplankton-Zooplankton-Detritus (NPZD)-ecosystem model has been configured for the Benguela upwelling system. The model variables are dissolved nutrients, the two trophic levels phytoplankton and zooplankton and dead particulate organic matter, i.e. detritus (for details on this class of ecosystem models see Fennel & Neumann (2004)). This food chain is truncated at the trophic level of zooplankton. The model includes higher trophic levels (e.g. fish) only implicitly as part of the zooplankton mortality rate. In detail the state variables of the model are: three phytoplankton functional types, three zooplankton functional types, detritus that sinks through the water column, and sedimented detritus on the sea floor. Furthermore, the model explicitly represents the nutrients nitrate, ammonium, phosphate, but also dinitrogen, elements of the sulfur cycle (hydrogen sulfide, elemental sulfur) and oxygen. Unlike phytoplankton or zooplankton, the prokaryotes responsible for detritus mineralisation are no explicit model variables but are assumed to be omnipresent. The relevant metabolic process mediated by them are implemented and solely the environmental conditions define their metabolic rates. A schematic representation of the model compartments and flows between them is shown in Figure (2.1).

All chemical and biological variables are treated as Eulerian variables. They are represented as passive tracers that undergo the same physical advection and mixing as temperature and salinity. The dynamic equations for these quantities contain biological source and sink terms describing all ecological activities (e.g. mortality, grazing) and metabolic reactions (e.g. nutrient assimilation, mineralisation of organic matter).

The model follows the cycling of nitrogen through the ecosystem. The units of most state variables are aqueous concentrations of nitrogen expressed in $mol\,kg^{-1}$. Hence, the biomass of the organisms is represented by e.g. 'Nitrogen in zooplankton' and the detritus variable is 'Nitrogen in detritus'.

The modeled phytoplankton is represented by following functional types,

- larger cells, fast growing at nutrient rich conditions which are sinking and may leave the euphotic zone and herein after referred to as 'Diatoms',

- smaller cells with a competitive advantage at lower nutrient concentrations and herein after referred to as 'Flagellates',

- and diazotrophs which are able to fix atmospheric dinitrogen gas (N_2). The inherent buoyancy of these organisms resulting from intracellular gas vacuoles is also included and herein after referred to as 'Cyanobacteria'.

Model studies of Deutsch et al. (2007) suggest that dinitrogen-fixation is closely coupled to upwelling regions where denitrification takes place. The Benguela upwelling system is one of the areas where Deutsch et al. (2007) predict high dinitrogen-fixation rates. Indeed,

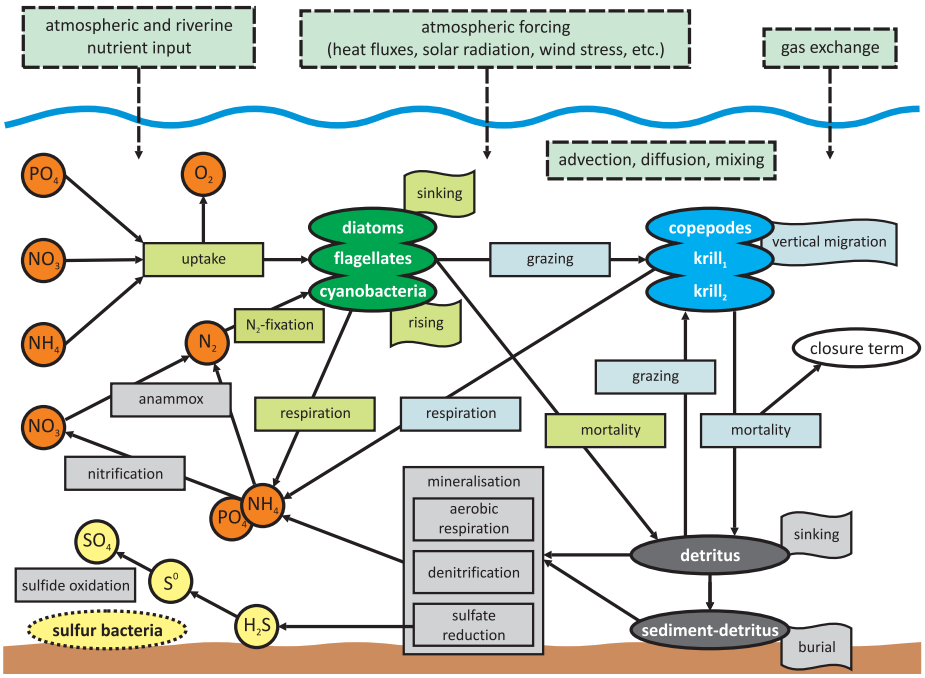

Fig. 2.1
Conceptual diagram of the nitrogen-based ecosystem model. State variables are denoted by ellipses (organisms) and circles (nutrients), processes by rectangular boxes and banners, flows with arrows and physical processes with dashed lines. Also sulfur bacteria are depicted on the sediment surface despite not beeing an explicit model variable. For the sake of simplicity, not all nutrient fluxes are shown. For instance, oxygen, nitrate or sulfate consumption in aerobic and anaerobic mineralisation of detritus are not displayed.

Abb. 2.1
Konzeptionelles Diagramm des stickstoffbasierten Ökosystemmodells. Zustandsvariablen sind als Ellipsen (Organismen) und Kreise (Nährstoffe) dargestellt, Prozesse als Rechtecke und Fähnchen, Flüsse als Pfeile und physikalische Prozesse als gestrichelte Linien. Auch das Wachstum von Schwefelbakterien auf der Sedimentoberfläche ist im Modell implementiert. Der Einfachheit halber sind nicht alle Nährstoffflüsse dargestellt. Das betrifft zum Beispiel, Sauerstoff-, Nitrat- oder Sulfatverbrauch durch die aerobe und anerobe Mineralisierung von Detritus.

Sohm et al. (2011) measured substantial rates of 85 $\mu mol\, m^{-2}\, d^{-1}$. The authors could only partly identify unicellular cyanobacteria responsible for this activity, otherwise the presence of unknown heterotrophic diazotrophs was suggested. In our model only diazotroph cyanobacteria are implemented as a separate functional phytoplankton type.

Zooplankton is the next trophic level, i.e. these organisms graze on phytoplankton, but may do so also on zooplankton and on detritus. The modeled zooplankton is represented by following functional types,

- herbivorous mesozooplankton with a high temperature optimum, not performing diel vertical migration and herein after referred to as 'Copepodes',

- herbivorous macrozooplankton with a high temperature optimum, performing diel vertical migration on a very regular basis and typical on the continental shelf and slope and herein after referred to as 'Krill 1',

- carnivorous macrozoolankton with a lower temperature demand, almost permanently found at depth and with a high tolerance to depleted oxygen conditions and herein after referred to as 'Krill 2'.

All dead organisms turn into detritus. Detritus sinks down and is either grazed by zooplankton or is mineralised by the metabolic activity of prokaryotes releasing phosphate and ammonium. Depending on the redox conditions and the availability of terminal electron acceptors (i.e. oxygen, nitrate, sulfate) in the water column different mineralisation processes dominate (Tab. 2.1). Part of the 'Detritus' may reach the sea floor and is there accumulated as 'Sediment-detritus'. The sediment-detritus is also mineralised by prokaryotes. However, if a certain thickness of the sediment is reached, all sediment below this layer is considered as buried. Buried detritus and nutrients are not recycled to the water column as long as a resuspension event eventually diminishes the thickness of the sediment layer.

All metabolic processes implemented in the model are listed in Table (2.1). Their stoichiometry are described in detail in the following sections 2.3.2-2.3.10.

Tab. 2.1
Metabolic processes implemented in the model.

Tab. 2.1
Metabolische Prozesse, die im Modell implementiert sind.

Metabolic processes	**Section**
Photoautotrophic nitrate and ammonium assimilation	2.3.2
Dinitrogen fixation	2.3.3
Chemolithoautotrophic nitrification	2.3.4
Heterotrophic oxygen respiration	2.3.5
Heterotrophic denitrification (nitrate respiration)	2.3.6
Heterotrophic sulfate reduction (sulfate respiration)	2.3.7
Anaerobic ammonium oxidation (Anammox)	2.3.8
Chemolithoautotrophic sulfide oxidation	2.3.10

2.2 Notation

All chemical compounds are represented by their chemical formulas. The concentration of the compound in $[mol\,kg^{-1}]$ is specified by the notation to place the formula of the compound in square brackets. For organic matter, this notation is too complex and the following abbreviations are used:

- OM stands for nitrogen in organic matter,

- P_i stands for nitrogen in phytoplankton of the functional group i,
- Z_j stands for nitrogen in zooplankton of the functional group i,
- D stands for nitrogen in detritus,
- SD stands for nitrogen in sediment-detritus.

The abbreviations in square brackets, i.e. $[OM]$, $[P_i]$, $[Z_j]$ and $[D]$ refer to concentrations in moles per volume, while $[SD]$ stands for amount of nitrogen in sediment per area.

2.3 Stoichiometries of metabolic processes

2.3.1 Stoichiometry of organic matter and dissolved nutrients

Following formula represents the particulate organic matter (organisms and detritus) in the model:

$$(CH_2O)_{106}(NH_3)_{16}(H_3PO_4). \tag{2.1}$$

Thus, the stoichiometry of organic matter strictly follows the Redfield carbon:nitrogen:phosphorus ratio of 106:16:1. Furthermore, nitrogen flux between organisms by grazing results in a corresponding Redfield phosphorus and carbon flux. Following stoichiometry is valid:

$$s_1 = \frac{[P]}{[N]} = \frac{1}{16} = 0.0625; \qquad s_2 = \frac{[C]}{[N]} = \frac{106}{16} = 6.625. \tag{2.2}$$

In contrast, the dissolved nutrient concentrations in the seawater are explicitly considered as model variables, i.e. they are not coupled and the ratios may depart from the Redfield ratio. Microbial metabolism (e.g. nitrogen-fixation, denitrification, Anammox) drives dissolved nutrient ratios away from the Redfield ratio (Arrigo, 2005). These shifts can be quantified with the current model.

2.3.2 Photoautotrophic nitrogen assimilation by phytoplankton

Photoautotrophic phytoplankton use the energy from sunlight to convert carbon dioxide and water into organic matter. The oxygen release from photosynthesis links the oxygen dynamics with the carbon cycle,

$$6\,CO_2 + 6\,H_2O \overset{h\nu}{\rightarrow} C_6H_{12}O_6 + 6\,O_2. \tag{2.3}$$

As the model is a nitrogen-based ecosystem model, growth of photoautotrophic phytoplankton is not defined as the rate of carbon dioxide fixation but of nitrogen assimilation. The molecular Redfield ratio of carbon:nitrogen of 106:16 is applied in this model to obtain the uptake of nitrogen from the uptake of carbon by phytoplankton.

Both ammonium and nitrate are assimilated by phytoplankton in the model. Nitrate is the far most abundant nitrogen source in the ocean and Wasmund et al. (2005) or Rees et al. (2006) determined nitrate and ammonium concentrations within the Benguela upwelling system of 10-33 μM and 0.1-0.3 μM, respectively. No explicit preference for a nitrogen source

is implemented and organic nitrogen compounds such as urea or amino acids are not considered.

The gross reaction for the production of organic matter with ammonium as the nitrogen source is:

$$106\,CO_2 + 16\,NH_3 + H_3PO_4 + 106\,H_2O \rightarrow (CH_2O)_{106}(NH_3)_{16}(H_3PO_4) + 106\,O_2. \tag{2.4}$$

Alternatively, if nitrate is utilised, additional oxygen is released from the reduction of nitrate to ammonium:

$$106\,CO_2 + 16\,HNO_3 + H_3PO_4 + 122\,H_2O \rightarrow (CH_2O)_{106}(NH_3)_{16}(H_3PO_4) + 138\,O_2. \tag{2.5}$$

The released oxygen in terms of assimilated nitrogen (as nitrate and ammonium) or in terms of nitrogen in phytoplankton is given by:

$$s_3 = \frac{[O_2]}{[NH_3]} = \frac{[O_2]}{[P_i]} = \frac{106}{16} = 6.625. \tag{2.6}$$

$$s_4 = \frac{[O_2]}{[HNO_3]} = \frac{[O_2]}{[P_i]} = \frac{138}{16} = 8.625. \tag{2.7}$$

In the model, the phytoplankton functional groups 'Diatoms' and 'Flagellates' assimilate both nitrate and ammonium. In contrast, 'Cyanobacteria' perform biological dinitrogen fixation, i.e. first convert dinitrogen to ammonium and subsequently assimilate it (see also 2.3.3).

2.3.3 Dinitrogen fixation by diazotrophs

Although dinitrogen gas (N_2) is the most abundant species of nitrogen in seawater, it is inaccessible for most phytoplankton. Diazotrophs, mainly a few members of the cyanobacteria, are unique in that they are capable of converting dinitrogen to ammonium in a process called biological dinitrogen fixation:

$$N_2 + 8\,H^+ + 8\,e^- \rightarrow 2\,NH_3 + H_2. \tag{2.8}$$

Subsequently, cyanobacteria assimilate ammonium. In contrast to other phytoplankton, growth of diazotrophic cyanobacteria is not limited by nitrate or ammonium but by the availability of phosphate as the second essential nutrient.

2.3.4 Chemolithoautotrophic nitrification

Oceanic nitrification is the biological oxidation of ammonia to nitrate in two steps, i.e. ammonia oxidation to nitrite and nitrite oxidation to nitrate. These processes are mediated by groups of ammonia-oxidizing bacteria and nitrite-oxidizing bacteria, respectively. Both are strictly aerobic chemoautotrophic organisms that actively convert inorganic carbon into biomass.

Following net chemical equation of nitrification is implemented in the model:

$$NH_3 + 2\,O_2 \rightarrow HNO_3 + H_2O. \tag{2.9}$$

Accordingly, nitrification links the oxygen and nitrogen cycle with following stoichiometric ratio of oxygen and ammonium:

$$s_5 = \frac{[O_2]}{[NH_3]} = \frac{2}{1} = 2.000. \tag{2.10}$$

2.3.5 Heterotrophic oxygen respiration: cellular respiration and respiration of organic matter

Phytoplankton and zooplankton can only thrive in oxic environments where they respire by using oxygen. Oxygen respiration is also the most efficient way of mineralising organic matter by prokaryotes. This process produces ammonium and is the reverse reaction of the ammonium assimilation (see 2.3.2):

$$\begin{aligned}(CH_2O)_{106}(NH_3)_{16}(H_3PO_4) + 106\,O_2 \rightarrow \\ 106\,CO_2 + 16\,NH_3 + H_3PO_4 + 106\,H_2O.\end{aligned} \tag{2.11}$$

Thus, aerobic dissimilation links the oxygen and nitrogen cycle with following stoichiometric ratio of oxygen and ammonia in organic matter:

$$s_6 = \frac{[O_2]}{[NH_3]} = \frac{[O_2]}{[OM]} = \frac{106}{16} = 6.625. \tag{2.12}$$

2.3.6 Heterotrophic denitrification of organic matter

If dissolved oxygen becomes depleted (suboxic or anoxic conditions, $[O_2] < 5\,\mu M$), organic matter is mineralised in anaerobic processes involving alternative terminal electron acceptors in lieu of oxygen. If nitrate is present, it acts as the terminal electron acceptor and denitrification becomes dominant. Denitrification is regarded as the major mineralisation pathway of detritus in the OMZs of the ocean, including the Benguela upwelling system (Tyrrell & Lucas, 2002).

Denitrification is a stepwise reduction process where nitrate is reduced to dinitrogen *via* the intermediates nitric oxide and nitrous oxide:

$$NO_3^- \rightarrow NO_2^- \rightarrow NO \rightarrow N_2O \rightarrow N_2. \tag{2.13}$$

As long as the nitrogen species are linked by a linear sequence of enzymatic reactions, as it is the case for denitrification, it is possible to define new model variables, e.g. 'nitrite + nitrate', that represent both compounds. As the nitrite concentration in the seawater is generally small ($< 3\,\mu M$) (Nicholls et al., 2007), it is assumed that nitrate reduction to nitrite is fast and not limiting and all nitrite-related processes in the model are approximately parametrized in terms of nitrate. However, the marine nitrogen cycle is not a linear pathway and implementing processes like anaerobic ammonium-oxidation (Anammox) needs to consider several reaction pathways to nitrite (Voss & Montoya, 2009). The explicit calculation of nitrite in the model was only avoided with some strong simplification (see 2.3.8).

Following net equation for denitrification of organic matter is implemented in the model Stigebrandt & Wulff (1987):

$$\begin{aligned}(CH_2O)_{106}(NH_3)_{16}(H_3PO_4) + 84.8\,HNO_3 \rightarrow \\ 106\,CO_2 + 16\,NH_3 + H_3PO_4 + 42.4\,N_2 + 148.4\,H_2O.\end{aligned} \tag{2.14}$$

Accordingly, the amount of nitrate consumed to mineralise detritus is given by:

$$s_7 = \frac{[HNO_3]}{[D]} = \frac{84.8}{16} = 5.300. \tag{2.15}$$

However, far less ammonium accumulates in the anoxic and suboxic water column than it would be expected from the stoichiometry of denitrification. It was already suggested by RICHARDS (1965) that part of the ammonium immediately oxidizes to free dinitrogen. Only recently, DALSGAARD ET AL. (2003) showed for anoxic waters of Golfo Dulce (Costa Rica) and KUYPERS ET AL. (2005) for the OMZ of the Benguela upwelling system that ammonium does indeed not accumulate in the anoxic waters until nitrate is depleted. The authors demonstrated a tight coupling between ammonium liberated during denitrification and further transformation by the Anammox process (see 2.3.8).

2.3.7 Heterotrophic sulfate reduction of organic matter

Due to high productivity in the ecosystem, both oxygen and nitrate are frequently depleted in the seawater causing a very specific sediment geochemistry on the Namibian shelf. Markedly high rates of sulfate reduction ($100\,mM\,a^{-1}$ of SO_4^{2-}) were measured from the sediment-water interface down to 10-15 cm sediment depth (BRÜCHERT ET AL., 2003; SCHÄFER ET AL., 2008). Sulfate is reduced to sulfide (S_2^-), typically in the form of dissolved hydrogen sulfide (H_2S) by sulfate-reducing prokaryotes.
Sulfate reduction takes place according to the overall reaction:

$$\begin{aligned}(CH_2O)_{106}(NH_3)_{16}(H_3PO_4) + 53\,H_2SO_4 \rightarrow \\ 106\,CO_2 + 16\,NH_3 + H_3PO_4 + 53\,H_2S + 106\,H_2O.\end{aligned} \tag{2.16}$$

The amount of hydrogen sulfide released from heterotrophic sulfate reduction in terms of nitrogen in detritus is:

$$s_8 = \frac{[H_2S]}{[NH_3]} = \frac{53}{16} = 3.3125. \tag{2.17}$$

Sulfide is rapidly oxidised in the water column (see 2.3.9, WRIGHT ET AL. (2012)).

2.3.8 Anaerobic ammonium oxidation (Anammox)

For decades, denitrification has been the only know pathway for oceanic N_2 production. However, anaerobic ammonium-oxidation (Anammox) seems to account for between 25 and 50% of the total marine N_2 production (DEVOL, 2003; ARRIGO, 2005; KUYPERS ET AL., 2005). At hypoxic conditions ($[O_2] < 50\,\mu M$), ammonium and nitrite (NO_2^-) are converted with a stoichiometric ratio of 1:1 to yield N_2 (KUYPERS ET AL., 2005):

$$HNO_2 + NH_3 \rightarrow N_2 + 2\,H_2O. \tag{2.18}$$

Two microbial processes may lead to nitrite production and thus directly couple to Anammox: anaerobic nitrate reduction (denitrification) and aerobic ammonium oxidation (nitrification), the latter at hypoxic conditions (LAM ET AL., 2009).

In the model, nitrite converted in the Anammox process is obtained from an incomplete denitrification reaction:

$$(CH_2O)_{106}(NH_3)_{16}(H_3PO_4) + 212\,HNO_3 \rightarrow$$
$$106\,CO_2 + 16\,NH_3 + H_3PO_4 + 212\,HNO_2 + 106\,H_2O. \tag{2.19}$$

Accordingly, the amount of nitrite released by mineralisation of detritus in terms of nitrogen is given by:

$$s_9 = \frac{[HNO_2]}{[D]} = \frac{212}{16} = 13.250. \tag{2.20}$$

As described above (see 2.3.6), nitrite is approximately parametrized in terms of nitrate and Anammox is implemented in the model as a direct reaction of ammonium and nitrate (stoichiometric ratio of 1:1).

2.3.9 Chemolithoautotrophic sulfide oxidation in the water column

Sulfide released from heterotrophic sulate reduction (see 2.3.7) is efficiently oxidized with oxygen in the water column, even at very low oxygen concentrations. In the model, hydrogen sulfide is oxidised with oxygen in two steps *via* elemental sulfur:

$$2\,H_2S + O_2 \rightarrow 2\,S^0 + 2\,H_2O. \tag{2.21}$$

$$2\,S^0 + 3\,O_2 + 2\,H_2O \rightarrow 2\,H_2SO_4. \tag{2.22}$$

The processes are implemented in the model with following stoichiometric ratios:

$$s_{10} = \frac{[O_2]}{[H_2S]} = 0.500 \tag{2.23}$$

$$s_{11} = \frac{[O_2]}{[S]} = 1.500 \tag{2.24}$$

Additionally, sulfide oxidation is coupled with chemolithoautotrophic denitrification in the water column. Sulfide-oxidizing microorganisms are abundant in oxygen minimum zones (Wright et al., 2012), one example is the SUP05 cluster within the γ-proteobacteria (Walsh et al., 2009). In the model, hydrogen sulfide is oxidised with nitrate in two steps *via* elemental sulfur and a complete denitrification reaction to dinitrogen takes place:

$$5\,H_2S + 2\,HNO_3 \rightarrow N_2 + 5\,S + 6\,H_2O. \tag{2.25}$$

$$5\,S^0 + 6\,HNO_3 \rightarrow 3\,N_2 + 5\,H_2SO_4. \tag{2.26}$$

Both processes are implemented in the model with following stoichiometric ratios:

$$s_{12} = \frac{[HNO_3]}{[H_2S]} = 0.400 \tag{2.27}$$

$$s_{13} = \frac{[HNO_3]}{[S]} = 1.200 \tag{2.28}$$

2.3.10 Chemolithoautotrophic sulfide oxidation on the sediment surface

Sulfate reduction in the sediment as well as in near bottom waters produces high concentrations of dissolved hydrogen sulfide (H_2S). However and similar to the processes described for the water column, hydrogen sulfide at the sediment-water interface is efficiently reoxidized by chemolithoautotrophic sulfide-oxidizing bacteria, e.g. the large bacterium *Thiomargarita namibiensis* (Schulz et al., 1999) or the filamentous *Beggiatoa* and *Thioplaca* species (Preisler et al., 2007). These organisms thrive by oxidising H_2S with oxygen in oxic bottom water or otherwise with nitrate. It has been shown that nitrate is stored in vacuoles at concentrations up to 800 mM (Schulz et al., 1999), an adaptation that enables the bacteria to survive periods where nitrate is absent in the ambient environment.

If oxygen is available, sulfur bacteria prefer the energetically more favorable oxidation of hydrogen sulfide with oxygen. Only the complete oxidation of hydrogen sulfide to sulfate is implemented in the model:

$$H_2S + 2\,O_2 \rightarrow H_2SO_4. \tag{2.29}$$

This process has following stoichiometric ratio:

$$s_{14} = \frac{[O_2]}{[H_2S]} = 0.500 \tag{2.30}$$

In the absence of oxygen, benthic sulfide-oxidizing bacteria perform hydrogen sulfide oxidation with nitrate through the process of DNRA (dissimilatory nitrate reduction to ammonium) (Lam et al., 2009), i.e. nitrate is reduced to ammonium at a ratio of $1:1$. Sulfide is oxidised with nitrate first to elemental sulfur (S^0) and stored in globules that give the bacteria mats a white appearance. In a second step, elemental sulfur is further oxidised to sulfate. However, only the complete net oxidation of hydrogen sulfide to sulfate is implemented in the model according to:

$$H_2S + HNO_3 + H_2O \rightarrow NH_3 + H_2SO_4. \tag{2.31}$$

The oxidation of sulfide with nitrate implies following stoichiometry:

$$s_{15} = \frac{[HNO_3]}{[H_2S]} = \frac{1}{1} = 1.000. \tag{2.32}$$

In sediments of high productive upwelling systems, i.e. also on the Namibian shelf, microbial sulfide production can overwhelm the nitrate pool and hydrogen sulfide can accumulate in the sediment surface layer to $[H_2S] > 10\,mM$. Hydrogen sulfide is then released to the water column by diffusion and episodic gas eruptions (Lavik et al., 2009).

2.3.11 Summary of stoichiometric ratios

In summary, following stoichiometric ratios link the nitrogen cycle in the model with phosphor, oxygen and sulfur dynamics.

Tab. 2.2
Stoichiometric ratios to link nitrogen, phosphorus, oxygen and sulfur cycle in the model.

Tab. 2.2
Stöchiometrische Koeffizienten, mit denen die Stickstoff-, -Phosphor-, Sauerstoff- und Schwefelzyklen aneinander gekoppelt werden.

Constant	Nutrients	Value	Metabolic process
s_1	$P:N$	0.0625	Redfield phosphorus:nitrogen ratio of particulate organic matter
s_2	$C:N$	6.625	Redfield carbon:nitrogen ratio of particulate organic matter
s_3	$O_2:NH_3$	6.625	Ammonium assimilation of phytoplankton
s_4	$O_2:NO_3$	8.625	Nitrate assimilation of phytoplankton
s_5	$O_2:NH_3$	2.000	Nitrification
s_6	$O_2:NH_3$	6.625	Heterotrophic Oxygen respiration
s_7	$NO_3:NH_3$	5.300	Heterotrophic denitrification
s_8	$H_2S:NH_3$	3.3125	Heterotrophic sulfate reduction
s_9	$NO_2:NH_3$	13.250	Anammox
s_{10}	$O_2:H_2S$	0.500	Oxidation of hydrogen sulfide to elemental sulfur with oxygen in the water column
s_{11}	$O_2:S^0$	1.500	Oxidation of elemental sulfur to sulfate with oxygen in the water column
s_{12}	$NO_3:H_2S$	0.400	Oxidation of hydrogen sulfide to elemental sulfur with nitrate in the water column
s_{13}	$NO_3:S^0$	1.200	Oxidation of elemental sulfur to sulfate with nitrate in the water column
s_{14}	$O_2:H_2S$	0.500	Oxidation of hydrogen sulfide to sulfate with oxygen in the sediment
s_{15}	$NO_3:H_2S$	1.000	Oxidation of hydrogen sulfide to sulfate with nitrate in the sediment

3 Functional responses and dynamic equations

3.1 The generalized advection-diffusion equations

The dynamic equations for all passive tracers X (i.e. temperature, salinity, phytoplankton, zooplankton, etc.) in the model have the general form:

$$\frac{\partial [X]}{\partial t} = \mathcal{P}([X]) + \mathcal{S}([X]). \tag{3.1}$$

The operator $\mathcal{P}$ of the tracer X describes the physical processes as horizontal and vertical advection ($\mathcal{A}$), horizontal turbulent diffusion ($\mathcal{D}$), vertical turbulent diffusion ($\mathcal{F}_z^{turb}$) and optionally for particulate organic matter (i.e. phytoplankton, zooplankton and detritus) sinking with a specific velocity w_X^{sink} according to following equation:

$$\mathcal{P}([X]) = \mathcal{A}([X]) + \mathcal{D}([X]) - \frac{\partial \mathcal{F}_z^{turb}([X])}{\partial z} - \frac{\partial w_X^{sink}[X]}{\partial z} \tag{3.2}$$

The operator $\mathcal{S}$ describes all source and sink terms of the tracer X in the ecosystem. These are described in detail for each state tracer in Section 3.3 and are listed in Table 3.2.

Except of sinking of particulate organic matter, all other processes are maintained by the usual tracer schemes of *MOM-4*.

3.2 Specific physical processes affecting particulate organic matter

3.2.1 Sinking

Particulate organic matter may undergo a specific vertical movement. For sinking diatoms and detritus w_X^{sink} is negative, zooplankton may undergo a vertical migration, flagellates and cyanobacteria do not sink in the model.

The density of diatoms and detritus particles is assumed to be larger than that of the surrounding water. Thus, the diatoms and detritus have the tendency to sink to the bottom. The sinking velocity depends on particle size and density but may be also changed by aggregation of particles. Sinking of detritus removes available nitrogen from the surface waters. The sinking particles undergo mineralisation processes recycling nitrogen and phosphorus from organic compounds. Hence, the ratio of sinking velocity to the velocity of recycling is a critical quantity for the nutrient budget of the surface layer.

The estimation of the sinking velocity is complex and disputed in the literature. A constant sinking velocity for all particles has been assumed in applications for marginal seas (Fennel

& NEUMANN, 2004). For deep sea applications, in contrast, aggregation processes play an important role for detritus and the average sinking velocity becomes a complex function of depth but also from the surface size spectrum of particulate matter (KRIEST & OSCHLIES, 2007). A constant sinking velocity w_X^{sink} is considered as a reasonable approximation in the mixing surface layer, but this parameter increases with depth in the less turbulent deeper layers:

$$w_X^{sink}(z) = w_X^0(1 + a_X \frac{d^2}{z_h^2 + d^2}), \tag{3.3}$$
$$d = \mathsf{max}(z - h_{blt}, 0).$$

The parameter z_h is diagnosed from the mixing layer depth, h_{blt}, calculated by the K-profile vertical mixing scheme. At levels, z, below the mixing layer depth, d is the distance from the mixing layer. Within the mixing layer d is set to zero. To model sinking of detritus in the Benguela upwelling system, the parameterisations $z_h = 2\,h_{blt}$, $a_D = a_{Dia} = 2$ and $w_D^{sink,0} = -3\,m\,d^{-1}$ were chosen. Diatoms sink with $w_{Dia}^{sink,0} = -1\,m\,d^{-1}$.

To ensure zero surface fluxes of phytoplankton, zooplankton and detritus, the additional vertical movement must vanish at the sea surface but may differ from zero at the bottom as exchange with the model sediment is considered,

$$w_X^{sink} = 0, \qquad \text{for } z = \eta, \tag{3.4}$$
$$w_X^{sink}\,X + \mathcal{F}_z^{turb}(X) = -L_{X,S}\,X + L_{S,X}\,S, \qquad \text{for } z = -H. \tag{3.5}$$

Sedimentation and resuspension depend on the bottom stress caused by currents and waves. Here a simple scheme is invoked which assumes sedimentation if the shear bottom stress is smaller than a critical value but resuspension takes place if the bottom stress exceeds a critical value,

$$L_{X,S} = l_{X,S}\,\theta\,(\tau^{crit} - \tau)$$
$$L_{S,X} = l_{S,X}\,\theta\,(\tau - \tau^{crit}) \tag{3.6}$$

If the stress is below its critical value, the turbulent flux at the bottom becomes small and $w_X^{sink}(z = -H) \approx -l_{X,S}$ is a good approximation. Noticeably, the near bottom sinking velocity $w_X^{sink}(z = -H)$ may be smaller than in the water column and a so called fluffy layer may develop where detritus is accumulated but does not form a solid sediment. As a consequence, mineralisation takes place under water-column-like conditions and not like in the sediment. Although this layer cannot be resolved, a sedimentation velocity smaller than the sinking velocity $|l_{X,S}| < |w_X^{sink}|$ leads to enrichment of detritus in the bottom-most layer, which simulates some properties of a fluffy layer.

In the current implementation, only detritus is allowed to settle. Bioturbation may keep a certain amount of detritus in suspension. It is a process independent of the bottom stress but depends on the activity of benthic organisms. However, bioturbation is not implemented in the model yet. Also diatoms may sink eventually to the sea floor, but in contrast to detritus, diatoms remain in the lowest layer of the water column until they die (i.e. turn into detritus) or are lifted upward by vertical advective or turbulent fluxes. Thus, the boundary condition $w_X^{sink}(z = -H) = 0$, $\mathcal{F}_z^{turb}(X)(z = -H) = 0$ applies to diatoms.

3.2.2 Other tracer surface fluxes

At the surface, fluxes of nutrients X and oxygen from the atmosphere enter the system and at the bottom exchange with the sediment takes place,

$$\mathcal{F}_z^{turb}(X) = X^{flux}, \qquad \text{for } z = \eta, \tag{3.7}$$

$$\mathcal{F}_z^{turb}(X) = -B_{X,S} + B_{S,X} \qquad \text{for } z = -H. \tag{3.8}$$

Details on the processes near the sediment surface, which define $B_{X,S}$ and $B_{S,X}$, are described in section 3.5.

3.2.3 A note on time stepping and positive definiteness

With this complex set of coupled equations some programming measures are needed to keep the tracer concentrations positive. For a simple equation with a single source term

$$\frac{\partial X}{\partial t} = -CX, \tag{3.9}$$

the time step must be smaller than C^{-1} to get a positive definite solution for X. Because such a simple condition cannot be found for the complex system as described here a simple scheme to avoid negative tracer concentrations is implemented. First, the maximum reaction rates are calculated. If the consumed amount of a tracer exceeds the available amount of this quantity, the reaction rate is diminished to this value. However, this procedure may become critical for the model results if a single tracer can undergo modifications by several reactions. For instance, oxygen is consumed by cellular respiration of phytoplankton and zooplankton and during oxic mineralisation of detritus. In such case, the consecutive sequence of delimiting must be justified by the preference for one or the other reaction pathway.

3.3 Source and sink terms

The operator $\mathcal{S}$ of the advection-diffusion equations describes the specific source and sink terms of each model component. Table 3.1 summerises all implemented processes of the ecosystem model. The specific conversion rates $l_{X,Y}^{Z}$ can be understood as transformation of X to Y under the influence of Z (e.g. l_{D,NH_3}^{Den}: conversion of detritus to ammonium by denitrification). All source and sink terms of the single components are given in Table 3.2.

Phytoplankton equation. The source and sink terms related to a specific phytoplankton type P_i include growth R_i (i.e. increase of nitrogen in phytoplankton due to light-dependent nitrate and ammonium assimilation), cellular oxygen respiration l_{P,NH_3} (i.e. decrease of nitrogen in phytoplankton to ammonium), natural mortality $l_{P,D}$ (i.e. decrease of nitrogen in phytoplankton to detritus) and grazing by zooplankton G_i (i.e. loss of nitrogen in phytoplankton depending on the grazing pressure).

Zooplankton equation. The source and sink terms related to a specific zooplankton type (Z_j) include growth G_j (i.e. increase of nitrogen in zooplankton due to grazing of phytoplankton), cellular oxygen respiration l_{Z,NH_3} (i.e. loss of nitrogen in zooplankton to ammonium) and mortality $l_{Z,D}$ (i.e. loss of nitrogen in zooplankton to detritus). Both the respiration and the mortality terms consist of two components: the respiration (l_{Z,NH_3}^{resp}) and mortality ($l_{Z,D}^{nat}$) and

additionally excretion of dissolved and particulate organic matter during feeding ("molting" and "sloppy feeding", $l^{ex}_{Z,D}$ and l_{Z,NH_3}). Additionally, as the food web is truncated at the level of zooplankton, both rates of zooplankton loss terms include a quadratic closure term for the ecosystem model z^{clos} (see Section 3.4.2).

Suspended detritus equation. The variable detritus (D) summarises dead phytoplankton, dead zooplankton and faecal pellets. The two sources are described by the terms $l_{P,D}$, $l_{Z,D}$, mineralisation by prokaryotes is described by l_{D,NH_3} (i.e. loss of nitrogen in detritus to ammonium, sum of all aerobic and anerobic dissimilatory processes). Note, the bottom boundary condition for sinking detritus, Equation (3.5), that describes the transition from suspended detritus to sedimented detritus.

Tab. 3.1
Implemented processes in the ecosystem model.

Tab. 3.1
Implementierte Prozesse im Ökosystemmodell.

Abbreviation	**Process**
R_i	Growth of phytoplankton (i.e. primary production)
G_i	Growth of zooplankton (i.e. grazing)
l_{P,NH_3}	Cellular oxygen respiration of phytoplankton
$l_{P,D}$	Natural mortality of phytoplankton
$l_{Z,NH_3} = l^{resp}_{Z,NH_3} + l^{ex}_{Z,NH_3}$	Cellular oxygen respiration of zooplankton consisting of the respiration itself and ammonium excretion during grazing ("sloppy feeding")
$l_{Z,D} = l^{nat}_{Z,D} + l^{ex}_{Z,D}$	Mortality of zooplankton consisting of the natural mortality itself and excretion of particulate material during grazing ("sloppy feeding")
l_{NH_3,NO_3}	Nitrification: oxidation of ammonium to nitrate
l_{D,NH_3}	Total (aerobic and anaerobic) mineralisation of detritus
l^{Oxy}_{D,NH_3}	Oxygen respiration of organic matter
l^{Den}_{D,NH_3}	Heterotrophic denitrification of organic matter
l^{Sul}_{D,NH_3}	Heterotrophic sulfate reduction of organic matter
l^{Ana}_{D,NH_3}	Anaerobic ammonium oxidation of organic matter
$l^{O_2}_{H_2S,S}$, $l^{O_2}_{S,SO_4}$	Oxidation of hydrogen sulfide and elemental sulfur with oxygen
$l^{NO_3}_{H_2S,S}$, $l^{NO_3}_{S,SO_4}$	Oxidation of hydrogen sulfide and elemental sulfur with nitrate

Sedimented detritus equation. The variable detritus (SD) summarises sedimeneted dead phytoplankton, dead zooplankton and faecal pellets. $l_{D,SD}$ describes the source term.

All explicitly modeled nutrient variables of the ecosystem model (i.e. nitrate, ammonium, phosphate) as well as sulfur, hydrogen sulfide and oxygen are linked to the metabolic conver-

sions mediated by phytoplankton, zooplankton and prokaryotes. The equations for the nutrients contain the counterparts of the source and sink terms of the advection-diffusion equation for phytoplankton, zooplankton and detritus. The stoichiometric ratios s_x are derived in the respective Sections of 2.3.11 and are summerised in Tab. 2.2.

Nitrate equation. Nitrification is the only process in the modeled nutrient cycle where nitrate is built. Nitrate is consumed by two growing phytoplankton types (diatoms and flagellates, but not by cyanobacteria as they only fix dinitrogen), by denitrification, Anammox and by the chemical and biological oxidation of hydrogen sulfide and elemental sulfur with nitrate.

Ammonium equation. Ammonium is released by respiration of phytoplankton and zooplankton, as well as by prokaryotes mineralising detritus. Additionally, biological oxidation of hydrogen sulfide by sulfur bacteria on the sediment surface yields ammonium. These terms are the source terms of the ammonium-equation. Ammonium is consumed by two growing phytoplankton types (diatoms and flagellates, but not by cyanobacteria as they only fix dinitrogen), taken up by the nitrification process and by the anaerobic ammonium oxidation (Anammox).

Phosphate equation. In the model, the stoichiometry of all particulate organic matter (organisms and detritus) and the nutrient fluxes in the food web strictly follow the Redfield nitrogen:phosphorus ratio of 16:1. Accordingly, the source and sink terms of the phosphate equation are similar to the nitrate- and/or ammonium-equations. Respiration of phytoplankton, zooplankton and prokaryotes mineralising detritus release phosphate and are the source terms of the phosphate-equation. Phosphate is taken up by all three growing phytoplankton types (diatoms, flagellates, cyanobacteria).

Elemental sulfur equation. Both biological and chemical oxidation of hydrogen sulfide with nitrate and oxygen releases elemental sulfur and are the source terms of the sulfur-equation. Elemental sulfur can be further oxidized to sulfate, both by oxidation with oxygen and nitrate.

Hydrogen sulfide equation. Sulfate reduction releases hydrogen sulfide and is the only source term of the sulfide equation. According to the considerations of elemental sulfur, hydrogen sulfide is oxidised with oxygen and nitrate.

Oxygen equation. Apart from diffusion of oxygen from the atmosphere into the surface water, the release of oxygen from photosynthetic activity of phytoplankton is the exclusive source of dissolved oxygen and primary production links nitrogen with oxygen dynamics in the model. Accordingly, nitrate assimilation by diatoms and flagellates and ammonium assimilation by all phytoplankton functional groups, i.e. including cyanobacteria which first fix dinitrogen and subsequently assimilate ammonium. Cellular respiration of phytoplankton, zooplankton and mineralisation of detritus take up oxygen and are sink terms in the oxygen-equation. Additionally, nitrifying prokaryotes consume oxygen and chemical oxidation with oxygen of elemental sulfur and of hydrogen sulfide takes place.

Tab. 3.2
Source and sink terms of the components of the ecosystem model.

Tab. 3.2
Quell- und Senkterme der Zustandsvariablen des Ökosystemmodells.

Model component	**Equation**	
Phytoplankton	$\mathcal{S}([P_i]) =$	$R_i\,[P_i] - l_{P,NH_3}\,[P_i] - l_{P,D}\,[P_i] - G_j\,\frac{[P_i]}{[P_{sum}]}\,[Z_j]$
Zooplankton	$\mathcal{S}([Z_j]) =$	$G_j\,\frac{[Food_j]}{[Food_{sum}]}\,[Z_j] - l_{Z_j,NH_3}\,z^{clos}\,[Z_{sum}]^2 - l_{Z_j,D}\,z^{clos}\,[Z_{sum}]^2$
Detritus	$\mathcal{S}([D]) =$	$l_{P,D}[P_{sum}] + l_{Z,D}\,z^{clos}\,[Z_{sum}]^2 - l_{D,NH_3}\,[D] - G_j\,\frac{[D_i]}{[D_{sum}]}\,[Z_j]$
Nitrate	$\mathcal{S}([NO_3]) =$	$l_{NH_3,NO_3}[NH_3] - \frac{[NO_3]}{([NH_3]+[NO_3])}\sum_{i=1}^{2} R_i\,[P_i] - s_7\,l^{Den}_{D,NH_3}[D] - s_9\,l^{Ana}_{D,NH_3}[D] - s_{12}\,l^{NO_3}_{H_2S,S^0} - s_{13}\,l^{NO_3}_{S^0,SO_4}$
Ammonium	$\mathcal{S}([NH_3]) =$	$l_{P,NH_3}[P_{sum}] + l_{Z,NH_3}\,z^{clos}\,[Z_{sum}]^2 + l_{D,NH_3}\,[D] + s_{12}\,l^{NO_3}_{H_2S,S^0} + s_{13}\,l^{NO_3}_{S^0,SO_4} - \frac{[NH_3]}{([NH_3]+[NO_3])}\sum_{i=1}^{2} R_i\,[P_i] - l_{NH_3,NO_3}[NH_3] - s_9\,l^{Ana}_{D,NH_3}[D]$
Phosphate	$\mathcal{S}([PO_4]) =$	$s_1\,(l_{P,NH_3}[P_{sum}] + l_{Z,NH_3}\,m^{clos}\,[Z_{sum}]^2 + l_{D,NH_3}\,[D] - \sum R_i\,[P_i])$
Elemental sulfur	$\mathcal{S}([S^0]) =$	$s_{10}\,l^{O_2}_{H_2S,S^0} + s_{12}\,l^{NO_3}_{H_2S,S^0} - s_{11}\,l^{O_2}_{S^0,SO_4} - s_{13}\,l^{NO_3}_{S^0,SO_4}$
Hydrogen sulfide	$\mathcal{S}([H_2S]) =$	$s_8\,l^{SO_4}_{D,NH_3}\,[D] - s_{10}\,l^{O_2}_{H_2S,S^0} - s_{12}\,l^{NO_3}_{H_2S,S^0}$
Oxygen	$\mathcal{S}([O_2]) =$	$s_4\,\frac{[NO_3]}{([NH_3]+[NO_3])}\sum R_{1,2}\,[P_{1,2}] + s_3\,\frac{[NH_3]}{([NH_3]+[NO_3])}\sum R_i\,[P_i] - s_6\,l_{P,NH_3}[P_{sum}] - s_6\,l_{Z,NH_3}\,z^{clos}\,[Z_{sum}]^2 - s_6\,l^{Oxy}_{D,NH_3}\,[D] - s_5\,l_{NH_3,NO_3}[NH_3] - s_{10}\,l^{O_2}_{H_2S,S^0} - s_{11}\,l^{O_2}_{S^0,SO_4}$

3.4 Modeled processes in the water column

3.4.1 Phytoplankton-related processes

Underwater light field. Photoautotrophic phytoplankton growth is limited by photosynthetic active radiation (PAR) penetrating into the water column. The solar radiation at the sea surface (SR) varies with a large number of factors, including latitude, time of the day, time of the year and cloudiness. Solar radiation enters the model as a prescribed forcing field. A mean ratio of $PAR : SR = 0.50$ is applied in the model. In the water column, photosynthetic active radiation is absorbed by four major components: the water itself, dissolved yellow pigments, phytoplankton cells, and particulate matter such as e.g. detritus and faecal pellets. In the model, the attenuation of photosynthetic active radiation in the water column is given by using the approximate relationship:

$$PAR(z) = 0.5\, SR\, \exp(k_w z - k_c \int_z^0 dz'([P_{sum}] + [D]), \tag{3.10}$$

where z is the water depth and k_w and k_c are light attenuation coefficients of the water and due to particulate organic matter, respectively. Light attenuation depends on bulk phytoplankton P_{sum} and detritus D in the water column.

Light-dependent primary production. Light-dependent primary production is estimated from photosynthesis-light response curves. Additionally, the model includes the concept of photoacclimation of phytoplankton from Stigebrandt & Wulff (1987), i.e. cells exposed to low photosynthetic active radiation have a lower optimal irradiance for photosynthesis (I_{opt}) than cells exposed to high levels of photosynthetic active radiation. The optimal irradiance I_{opt} is simply set to 0.5 of PAR at the sea surface for all phytoplankton functional groups.

$$I_{opt} = \mathrm{max}(\frac{PAR}{2}, I_{min}), \tag{3.11}$$

Light-dependent primary production, $PP(I)$, of phytoplankton is implemented in the model by following functional response (Steele, 1962):

$$PP(I) = \frac{I}{I_{opt}} \exp(1 - \frac{I}{I_{opt}}). \tag{3.12}$$

where I_{min} is the minimal photosynthetic active radiation the phytoplankton can acclimate to and $I_{min,Dia} = 25\, W\, m^{-2}$, $I_{min,Fla} = 50\, W\, m^{-2}$ and $I_{min,Cya} = 50\, W\, m^{-2}$.

Similar to other functional responses of e.g. Platt et al. (1980); Webb et al. (1974); Walsby (1997), primary production increases linearly at low levels of photosynthetic active radiation, reaches a maximal value at I_{opt} and subsequently levels off.

Nutrient assimilation and growth of phytoplankton. Nutrient uptake is described with a modified Michaelis-Menten formula with squared arguments (Fennel & Neumann, 1996) which results in a sigmoid functional response. As the model strictly follows balanced phytoplankton growth, the Redfield ratio nitrogen:phosphorus ratio of 16:1 is also valid for nutrient assimilation of growing phytoplankton cells. Uptake of dissolved inorganic nitrogen,

$(NH_3 + NO_3)$, and phosphate, PO_4, reads:

$$Y(\alpha_i, ([NH_3] + [NO_3])) = \frac{([NH_3] + [NO_3])^2}{\alpha_i^2 + ([NH_3] + [NO_3])^2} \tag{3.13}$$
$$Y(s_1\,\alpha_i, [PO_4]) = \frac{[PO_4]^2}{s_1^2\alpha_i^2 + [PO_4]^2},$$

where α_i is the type-specific uptake efficiency for nitrogen and $\alpha_{Dia} = 6.00 \times 10^{-6}\, mol\, kg^{-1}$, $\alpha_{Fla} = 1.80 \times 10^{-6}\, mol\, kg^{-1}$, $\alpha_{Cya} = 2.25 \times 10^{-6}\, mol\, kg^{-1}$. The stoichiometric constant s_1 links nitrogen with phosphor uptake according to the Redfield ratio.

The nutrients ammonium, nitrate and phosphate as well as PAR limit growth of the phytoplankton types 'Diatoms' and 'Flagellates' according to the *Liebig law of the minimum*, i.e. growth depends on the element least in supply. Accordingly, the growth rates of 'Diatoms' and 'Flagellates' are defined as:

$$R_i = r_i^0 \min[Y(\alpha_i, [NH_3] + [NO_3]), Y(s_1\alpha_i, [PO_4]), PP(I)],$$

where $r_{Dia}^0 = 1.5\, d^{-1}$ and $r_{Fla}^0 = 0.8\, d^{-1}$ are the specific maximal growth rates for diatoms and flagellates, respectively.

For 'Cyanobacteria', in contrast, a temperature dependence of the growth rate, F^T, was chosen. It is also assumed that they only grow at temperatures $> 20°C$ (LaRoche & Breitbarth, 2005). As cyanobacteria can fix atmospheric nitrogen, they are assumed not to be limited by nitrate or ammonium:

$$R_{cya} = r_{cya}^0\, F^T \min[Y(s_1\alpha_3, [PO_4]), PP(I)], \tag{3.14}$$
$$F^T = \frac{1}{1 + \exp(T_{min} - T)},$$

where $r_{Cya}^0 = 0.6\, d^{-1}$ and $T_{min} = 20°C$.

Chlorophyll concentration in the water column. As chlorophyll is a common proxy of phytoplankton biomass, it is computed as an output variable of the model. Even though ratios of chlorophyll and phytoplankton biomass vary greatly among species and are affected nonlinearily by ambient nutrient, light, and temperatures (Geider et al., 1997; Li et al., 2010), a mean chlorophyll:carbon mass ratio ($m_{Chl,C}$) of 0.025 is implemented in the model. This is a strong simplification of Geider et al. (1997). It is also assumed that both phytoplankton $[P_{sum}]$ and detritus $[D]$ contain chlorophyll. These variables are converted into chlorophyll mass concentration $[Chl]$ with following parametrisation:

$$[Chl] = m_{Chl,C} \times 10^6 \times 12.0 \times s_2 \times ([P_{sum}] + [D]). \tag{3.15}$$

where $[Chl]$ is given in $mg\, m^{-3}$ and the chlorophyll : carbon mass ratio $m_{Chl,C} = 0.025$. The stoichiometric Refield ratio s_2 converts nitrogen in phytoplankton and detritus in $mol\, kg^{-1}$ into molar carbon-content according to the Redfield ratio, 12.0 in $g\, mol^{-1}$ is the molar mass of carbon.

Cellular oxygen respiration and mortality of phytoplankton. In the model, all phytoplankton types respire with the same and constant respiration rate $l_{P,NH_3} = 0.01\,d^{-1}$ and all types have the same and a constant mortality rate $l_{P,D} = 0.02\,d^{-1}$ at oxic conditions. However at suboxic conditions, i.e. dissolved oxygen concentrations $< 5\,\mu mol\,kg^{-1}$, mortality rate increases by a factor 10.

3.4.2 Zooplankton-related processes

Zooplankton grazing. The type III functional response for zooplankton feeding (Gentleman & Neuheimer, 2008) has been implemented in this model, and specifically the $Ivlev^2$-model. Grazing of zooplankton grows rapidly with food supply at low concentrations, but it is maximal at g^0. The Ivlev parameter Iv determines the steepness of the curve. Furthermore, growth (i.e. grazing) is assumed to be temperature-dependent and a temperature dependence of grazing F^T is parameterized according to Blanchard et al. (1996). The three zooplankton types implemented in this model are differentiated with respect to temperature dependence of grazing.

$$G = g^0\, F^T\, (1 - \, e^{(-Iv^2\,[Food]^2)}), \tag{3.16}$$

$$F^T = \left(\frac{T_{max} - T}{T_{max} - T_{opt}}\right)^{\beta} \; e^{\beta\left(\frac{T_{max}-T}{T_{max}-T_{opt}} - 1\right)}, \tag{3.17}$$

$$[Food] = [P_{sum}] + [Z_{sum}] + [D]. \tag{3.18}$$

where $g^{0,Cop} = 1.0\,d^{-1}$, $g^{0,Kr1} = 0.5\,d^{-1}$, $g^{0,Kr2} = 0.5\,d^{-1}$. $Iv = 1 \times 10^6\,kg\,mol^{-1}$ for all zooplankton types. Grazing is optimal at $T_{opt,Cop} = 15\,°C$, $T_{opt,Kr1} = 15\,°C$, $T_{opt,Kr2} = 10\,°C$. Grazing is inhibited at temperatures above $T_{max,Cop} = 25\,°C$, $T_{max,Kr1} = 25\,°C$, $T_{max,Kr2} = 15\,°C$. $\beta = 1.7$ is a dimensionless parameter and defines the steepness of the temperature dependence.

The three zooplankton types have different food preferences. The more herbivorous types 'Copepodes' and 'Krill 1' primarily feed on phytoplankton, but also on detritus and 'Krill 1' on smaller zooplankton. The carnivorous type 'Krill 2' primarily feeds on zooplankton, but also on detritus (Friedrich Buchholz, personal communication).

Tab. 3.3
Food preferences p_i of the zooplankton functional types.

Tab. 3.3
Nahrungspräferenzen p_i der funktionellen Zooplanktontypen.

Food item	**'Copepodes'**	**'Krill 1'**	**'Krill 2'**
p_{Dia}	0.39	0.29	0.00
p_{Fla}	0.39	0.29	0.00
p_{Cya}	0.02	0.02	0.00
p_{Det}	0.20	0.20	0.20
p_{Cop}	0.00	0.20	0.50
p_{Kr1}	0.00	0.00	0.20
p_{Kr2}	0.00	0.00	0.10

The food-dependent grazing rate of the two zooplankton types finally results from:

$$G_i = p_i\, G. \tag{3.19}$$

Cellular oxygen respiration, mortality and the closure term of zooplankton. Several studies have shown that not all of the grazed food is necessarily ingested and used for zooplankton growth (e.g. copepods: MOLLER (2005)). Grazing of zooplankton can considerably contribute to the microbial food web through the production of dissolved and particulate material from sloppy feeding, excretion and leakage from faecal pellets and molting. The respiration rate l_{Z,NH_3} of bulk zooplankton consists of a constant respiration rate itself, l^{resp}_{Z,NH_3}, and additionally of a grazing dependent part of ammonium excretion by zooplankton l^{ex}_{Z,NH_3}:

$$l_{Z,NH_3} = l^{resp}_{Z,NH_3} + l^{ex}_{Z,NH_3}, \tag{3.20}$$

$$l^{ex}_{Z,NH_3} = a_{ex,NH_3}\, G, \tag{3.21}$$

where $l^{resp}_{Z,NH_3,Cop} = 0.03\, d^{-1}$, $l^{resp}_{Z,NH_3,Kr1} = 0.01\, d^{-1}$ and $l^{resp}_{Z,NH_3,Kr2} = 0.01\, d^{-1}$. $a_{ex,NH_3} = 0.18$, i.e. 18% of the food is immediately excreted as dissolved ammonium. Additionally, the respiration rate l_{Z,NH_3} is reduced at hypoxic conditions ($< 60 \times 10^{-6}\, mol\, kg^{-1}$) by a the factor 10 and $l_{Z,NH_3} = 0$ at suboxic concentrations ($< 5 \times 10^{-6}\, mol\, kg^{-1}$).

The mortality rate of zooplankton consists of the natural mortality rate $l^{nat}_{Z,D}$ and a grazing dependent contribution to detritus due to excretion of particulate material, $l^{ex}_{Z,D}$:

$$l_{Z,D} = l^{nat}_{Z,D} + l^{ex}_{Z,D}, \tag{3.22}$$

$$l^{ex}_{Z,D} = a_{ex,D}\, G, \tag{3.23}$$

where $l^{nat}_{Z,D,Cop} = 0.03\, d^{-1}$, $l^{nat}_{Z,D,Kr1} = 0.01\, d^{-1}$ and $l^{nat}_{Z,D,Kr2} = 0.01\, d^{-1}$. $a_{ex,D} = 0.18$, i.e. 18% of the food is immediately excreted as particulate organic matter (detritus). Additionally, the mortality rate $l_{Z,D}$ is increased at suboxic conditions ($< 5 \times 10^{-6}\, mol\, kg^{-1}$) by a the factor 10.

Zooplankton is the highest trophic level of the food web that is explicitly modelled. This requires that the rate of zooplankton mortality due to consumption by higher predators is represented by some mathematical function that does not explicitly depend upon the population level of the higher predators, since such predators are not being modelled. This function is the zooplankton closure term z^{clos} and determines both the respiration term l_{Z,NH_3} and the mortality term $l_{Z,D}$. A quadratic term has been chosen:

$$\frac{\partial [Z_i]}{\partial t} = ... - l_{Z,NH_3}\, z^{clos}\, [Z]^2 - l_{Z,D}\, z^{clos}\, [Z]^2 \tag{3.24}$$

where $z^{clos} = 6.67 \times 10^5\, kg\, mol^{-1}$.

Diel vertical migration of zooplankton. Diel vertical migration (DVM) of zooplankton refers to a pattern of large vertical movements that are undertaken each day by these organisms. In the model, DVM is determined by following factors: (1) zooplankton sinks passively, but swims upward actively and does some random movement otherwise, (2) foraging opportunities (i.e. food gradients) and (3) environemntal factors (i.e. temperature, oxygen concentration,

hydrogen sulfide concentration and light). The three zooplankton types implemented in this model behave differently. 'Krill 1' and 'Krill 2' perform both DVM on a very regular basis, while the herbivorous 'Copepodes' are almost permanently found in the euphotic surface water. The following rules are applied in this model and are used as the basis for a numerical scheme for the calculation of the zooplankton migration velocity:

An implicit scheme is required to implement DVM of zooplankton. It is treated as the implicit vertical mixing that is done in *MOM-4* using a tridiagonal matrix solver (PRESS ET AL., 1992). Mixing and advection of a tracer T in level k is implemented like follows:

$$\begin{aligned} T_k =& T_k^n + \frac{\Delta t}{\Delta z t_k}(w_k^+ T_{k+1} + w_k^- T_k - w_{k-1}^+ T_k - w_{k-1}^- T_{k-1} \\ &+ \frac{\nu_k (T_{k+1} - T_k)}{\Delta z w_k} + \frac{\nu_{k-1}(T_{k-1} - T_k)}{\Delta z w_{k-1}}), \end{aligned} \tag{3.25}$$

with the upward and downward velocities:

$$\begin{aligned} w_k^+ &= 0.5\,(w_k + |w_k|) \\ w_k^- &= 0.5\,(w_k - |w_k|) \end{aligned}$$

and turbulent vertical mixing coefficient ν. Superscript n denotes the previous time level. For an implicit scheme this equation can be rewritten to

$$\begin{aligned} T_k^n =& T_k(1 + e_k + e_{k-1} - \omega_k^- + \omega_{k-1}^+) \\ &+ T_{k+1}(-e_k - \omega_k^+) + T_{k-1}(-e_{k-1} + \omega_{k-1}^-), \end{aligned} \tag{3.26}$$

with the abbreviations

$$\begin{aligned} e_k &= \frac{\Delta t}{\Delta z t_k}\frac{\nu_k}{\Delta z w_k} \\ \omega_k^+ &= \frac{\Delta t}{\Delta z t_k} w_k^+ \\ \omega_k^- &= \frac{\Delta t}{\Delta z t_k} w_k^-. \end{aligned} \tag{3.27}$$

This is a tridiagonal matrix equation of the form:

$$\begin{pmatrix} b_1 & c_2 & 0 & 0 & \dots & & & \\ a_2 & b_2 & c_3 & 0 & \dots & & & \\ 0 & a_3 & b_3 & c_4 & \dots & & & \\ \dots & & & & & & & \\ 0 & 0 & 0 & 0 & \dots & a_{k-1} & b_{k-1} & c_k \\ 0 & 0 & 0 & 0 & \dots & 0 & a_k & b_k \end{pmatrix} \begin{pmatrix} T_1 \\ T_2 \\ T_3 \\ \dots \\ T_{k-1} \\ T_k \end{pmatrix} = \begin{pmatrix} T_1^n \\ T_2^n \\ T_3^n \\ \dots \\ T_{k-1}^n \\ T_k^n \end{pmatrix}, \tag{3.28}$$

with

$$\begin{aligned} a_k &= -e_{k-1} + w_{k-1}^- \\ b_k &= 1 + e_k + e_{k-1} - w_k^- + w_{k-1}^+ \\ c_k &= -e_k - w_k^+. \end{aligned}$$

The subroutine *invtri* of *MOM-4* was modified to solve this matrix equation for T_k.

To find the migration velocity the following parameterisation is used to evaluate the various environmental factors:

- The two zooplankton types 'Krill 1' and 'Krill 2' intermittently sink passively with $w_{Z,Kr1}^{sink,0} = -800\,m\,d^{-1}$ and $w_{Z,Kr2}^{sink,0} = -600\,m\,d^{-1}$. They swim actively upward with $w_{Z,Kr1}^{rise,0} = 1600\,m\,d^{-1}$ and $w_{Z,Kr2}^{rise,0} = 1200\,m\,d^{-1}$. The net movement depends on the environment.

- Both zooplankton types avoid radiation exceeding $I(z) > I_{max}$ with $I_{max,Kr1} = 1.0 \times 10^{-20}\,mol\,photons\,m^{-2}\,s^{-1}$ and $I_{max,Kr2} = 1.0 \times 10^{-10}\,mol\,photons\,m^{-2}\,s^{-1}$. This behaviour is described by a cost function Θ_I that ranges between 0 and 1 and $\Theta_I = 1$ if the zooplankton is in the dark.

$$\Theta_I = \frac{I_{max}^2}{I(z)^2 + I_{max}^2}$$

- Zooplankton tends to rise at a minimum dissolved oxygen concentration $[O_{2,min}] = 5.0 \times 10^{-6}\,mol\,kg^{-1}$ and a maximum hydrogen sulfide concentration $[H_2S_{max}] = 1.0 \times 10^{-6}\,mol\,kg^{-1}$, expressed by the cost functions Θ_O and Θ_{H_2S}. $\Theta_O = 1$ and $\Theta_{H_2S} = 1$ if oxygen is depleted and hydrogen sulfide occurs, respectively.

$$\Theta_O = \frac{[O_{2,min}]^2}{[O_2(z)]^2 + [O_{2,min}]^2}$$
$$\Theta_{H_2S} = \frac{[H_2S_{max}]^2}{[H_2S(z)]^2 + [H_2S_{max}]^2}$$

- Both zooplankton types prevent to migrate into a water layer of a maximal temperature T_{max} and the cost function Θ_T ranges between 0 and 1.

$$\Theta_T = \frac{(T - T_{opt})}{(T_{max} - T_{opt})}$$

- For small food concentration, zooplankton follows the food gradient between the two depth layers k and $(k-1)$, i.e. $[Food_{(k-1)}] - [Food_{(k)}]$. For large food concentration it moves randomly.

$$\Theta_F = ([Food_{(k-1)}] - [Food_{(k)}])\,Iv\,e^{(-Iv^2\,[Food]^2)}$$

The resulting vertical zooplankton movement is a superposition of passive sinking and active rising triggered by darkness or low oxygen conditions and modified by the food gradient and some randomness.

$$w_Z = min((\Theta_O + \Theta_I), \Theta_T, 1)\left(w_Z^{rise,0}(1 + \Theta_F)\right) + w_Z^{sink,0}.$$

3.4.3 Chemolithoautotrophic nitrification

Until relatively recently, nitrification, i.e. oxidation of ammonium to nitrate, was believed to occur almost entirely at depth, possibly because of inhibition by light. However, YOOL ET AL. (2007) showed that a substantial fraction takes place near the surface. In the model, nitrification rate depends primarily on temperature, F^T, and a steep exponential increase is assumed. Nitrification only takes place if oxygen is available. The oxygen dependence, F^{O_2}, is a saturation function with a steep increase at hypoxic conditions, i.e. dissolved oxygen

concentrations $< 30 \times 10^{-6}\, mol\, kg^{-1}$. Nitrification is almost independent from dissolved oxygen at higher concentrations.

$$l_{Nit} = k^0_{Nit}\, F^T\, F^{O_2}, \tag{3.29}$$

$$F^T = e^{\beta_{Nit}\, T}, \tag{3.30}$$

$$F^{O_2} = \frac{[O_2]}{\alpha_{Nit} + [O_2]}, \tag{3.31}$$

with $k^0_{Nit} = 0.03\, d^{-1}$ and $\beta_{Nit} = 0.11\, K^{-1}$ which is equivalent to $Q_{10} = 3$ of the van 't Hoff rule, i.e. nitrification rate increases by factor 3 when temperature increases by $10\, K$. The parameter $\alpha_{Nit} = 3.75 \times 10^{-6}\, mol\, kg^{-1}$ is the half-saturation constant of the oxygen-dependence.

3.4.4 Mineralisation of detritus in the water column

Detritus is mineralised by a large suite of prokaryotes under oxic, hypoxic or anoxic conditions and ammonium is released in these heterotrophic processes. Even though the model does consider a strict threshold between oxic and suboxic conditions ($5 \times 10^{-6}\, mol\, kg^{-1}$), this concentration is not applied directly to define the contribution of aerobic and anaerobic mineralisation processes. Instead, the redox conditions and the availability of terminal electron acceptors (i.e. oxygen, nitrate, sulfate) are examined and the four mineralisation processes (i.e. oxygenic respiration, denitrification, sulfate reduction, and a certain amount of mineralisation by Anammox) are implemented *via* a smoothed step function (see below in this section, Equation 3.47).

The total mineralisation rate l_{D,NH_3} is the sum of the four mineralisation processes:

$$l_{D,NH_3} = l^{Oxy}_{D,NH_3} + l^{Den}_{D,NH_3} + l^{Sul}_{D,NH_3} + l^{Ana}_{D,NH_3}. \tag{3.32}$$

where l^{Oxy}_{D,NH_3} is mineralisation by oxygenic respiration, l^{Den}_{D,NH_3} by denitrification, l^{Sul}_{D,NH_3} by sulfate reduction and l^{Ana}_{D,NH_3} by Anammox.

Even though Anammox contributes to the total mineralisation rate, this process is considered as an additional 'bonus pathway' of detritus mineralisation. This is due to the assumption that the nitrite consumed by Anammox bacteria is produced in an incomplete denitrification reaction (see Equation 2.19). Accordingly, the mineralisation rate of the Anammox process is treated separately. The sum of only the three mineralisation processes oxygenic respiration, denitrification, sulfate reduction l^*_{D,NH_3} is temperature dependent and the following parameterisation is used:

$$l^*_{D,NH_3} = k^0_{D,NH_3}\, F^T, \tag{3.33}$$

$$F^T = e^{\beta_{min}\, T}, \tag{3.34}$$

with $k^0_{D,NH_3} = 0.003\, d^{-1}$ and $\beta_{min} = 0.0693\, K^{-1}$ which is equivalent to $Q_{10} = 2$ of the van 't Hoff's rule, i.e. mineralisation rate increases by factor 2 when temperature increases by $10\, K$.

The Anammox reaction rate also depends on temperature and is limited by the availability of

ammonium and nitrite and is inhibited at oxic conditions or if hydrogen sulfide is present:

$$l^{Ana}_{D,NH_3} = k^0_{Ana}\, F^T\, F^{O_2}\, F^{H_2S}\, F^{NH_3}\, F^{NO_2}, \tag{3.35}$$

$$F^T = \left(1 + \exp\frac{(T - 30\,°C)}{2}\right)^{-1} \left(1 + \exp\frac{(7\,°C - T)}{2}\right)^{-1}, \tag{3.36}$$

$$F^{O_2} = 1 - f_{O_2}, \tag{3.37}$$

$$F^{H_2S} = 1 - f_{H_2S}, \tag{3.38}$$

$$F^{NH_3} = f_{NO_3}, \tag{3.39}$$

$$F^{NO_2} = f_{NH_3}, \tag{3.40}$$

with $k^0_{Ana} = 0.02\,d^{-1}$ and the f-factors of the smoothed step function are given by Equations (3.47).

The consumed amount of nitrate and the released amount of nitrite in the incomplete denitrification is $-s_9\, l^{Ana}_{D,NH_3}\,[D]$. It is converted immediately with the same amount of ammonium to dinitrogen.

$$\begin{aligned} \Delta[NO_3]^{Ana} &= -s_9\, l^{Ana}_{D,NH_3}\,[D] \\ \Delta[NH_3]^{Ana} &= -s_9\, l^{Ana}_{D,NH_3}\,[D], \end{aligned} \tag{3.41}$$

where s_9 is the stoichiometric constant of the Anammox reaction.

Accordingly, the total amount of detritus mineralised in one time step is:

$$\begin{aligned} \Delta[D] &= l^*_{D,NH_3}[D]\Delta t + \Delta[D]^{Ana} \\ &= \Delta[D]^{Oxy} + \Delta[D]^{Den} + \Delta[D]^{Sul} + \Delta[D]^{Ana}. \end{aligned} \tag{3.42}$$

Preferred electron acceptors in the mineralisation of organic matter. If oxygen concentration is sufficient, aerobic prokaryotes are the most efficient recyclers of organic matter. If dissolved oxygen becomes depleted, organic matter is mineralised in anaerobic processes involving nitrate as the terminal electron acceptor. If nitrate becomes depleted, sulfate will be reduced. This strict order of consecutive oxidation steps has been implemented in the model. It is numerically expensive, but has the great advantage to be strictly positive definite if it is based on oxygen or nitrate of the new time level $\tau + \Delta t$.

First the redox conditions and the availability of terminal electron acceptors (i.e. oxygen, nitrate, sulfate) are examined.

- If oxygen is present, aerobic mineralisation (i.e. oxygen respiration) takes place.
- If nitrate is present but no oxygen and if the favored conditions for Anammox are not met, denitrification takes place.
- If no oxygen and no nitrate are present, sulfate reduction takes place.
- Anammox takes place at hypoxic conditions and if no hydrogen sulfate is present, but nitrate and ammonium are available.

This translates into following numerical scheme:

$$l^{Oxy}_{D,NH_3} = l_{D,NH_3}\, f_{O_2}, \tag{3.43}$$
$$l^{Den}_{D,NH_3} = l_{D,NH_3}\,(1 - f_{O_2}) f_{NO_3}\,(1 - f_{NH_3}(1 - f_{H_2S}))\,, \tag{3.44}$$
$$l^{Sul}_{D,NH_3} = l_{D,NH_3}\,(1 - f_{O_2})(1 - f_{NO_3}), \tag{3.45}$$
$$l^{Ana}_{D,NH_3} = l^{Ana}_{D,NH_3}\,(1 - f_{O_2}) f_{NO_3} f_{NH_3}(1 - f_{H_2S}), \tag{3.46}$$

where only the Anammox process is not defined as a specific proportion of the total mineralisation rate.

The delimiter f_X becomes 1 for high concentrations of X and 0 for very low concentrations. A mathematical function with favourable asymptotic characteristics has been developed. The parameter α determines the slope at $X = 0$. The choice of α depends on both, the metabolic properties of the prokaryotes and must quickly limit consumption of X at small concentrations to keep the numerical scheme positive:

$$f_X = \frac{1 - e^{-2\alpha X}}{1 + e^{-2\alpha X}} = \frac{2}{1 + e^{-2\alpha X}} - 1, \tag{3.47}$$

where $\alpha_{O_2} = 5.0 \times 10^5\, kg\, mol^{-1}$, $\alpha_{NH_3} = 2.2 \times 10^6\, kg\, mol^{-1}$, $\alpha_{NO_3} = 2.2 \times 10^6\, kg\, mol^{-1}$ and $\alpha_{H_2S} = 5.0 \times 10^3\, kg\, mol^{-1}$.

3.4.5 Oxidation of hydrogen sulfide and elemental sulfur in the water column

Both chemical and biological oxidation of hydrogen sulfide in the water column proceeds in two steps. First, hydrogen sulfide is oxidised to elemental sulfur, which can then be oxidised to sulfate. Both reactions may take place with dissolved oxygen or nitrate.

For numerical reasons, i.e. to get a positive definite scheme, an iterative calculation of the reaction rates is used. The first step is to calculate maximal conversion rates:

$$^{(1)}l^{O_2}_{H_2S,S^0} = k^{O_2,0}_{H_2S,S^0}\, F^T\, F^{O_2}\, [H_2S]\, [O_2], \tag{3.48}$$
$$^{(1)}l^{O_2}_{S^0,SO_4} = k^{O_2,0}_{S^0,SO_4}\, F^T\, F^{O_2}\, [S^0]\, [O_2], \tag{3.49}$$
$$^{(1)}l^{NO_3}_{H_2S,S^0} = k^{NO_3,0}_{H_2S,S^0}\, F^T\, F^{NO_3}\, [H_2S]\, [NO_3], \tag{3.50}$$
$$^{(1)}l^{NO_3}_{S^0,SO_4} = k^{NO_3,0}_{S^0,SO_4}\, F^T\, F^{NO_3}\, [S^0]\, [NO_3]. \tag{3.51}$$

with $k^{O_2,0}_{H_2S,S^0} = k^{NO_3,0}_{H_2S,S^0} = 8.0 \times 10^5\, d^{-1}$ and $k^{O_2,0}_{S^0,SO_4} = k^{NO_3,0}_{S^0,SO_4} = 2.0 \times 10^3\, d^{-1}$.

All oxidation reactions have the same exponential temperature dependence:

$$F^T = e^{\beta_{Sul}\, T}, \tag{3.52}$$

with $\beta_{Sul} = 0.0693\, K^{-1}$ which is equivalent to $Q_{10} = 2$ of the van 't Hoff rule, i.e. oxidation rates increase by factor 2 when temperature increases by $10\, K$.

As oxidation with oxygen is energetically more favourable than with nitrate, there is a strict preference for this reaction pathway to oxidise sulfide and sulfur:

$$F^{O_2} = 1, \tag{3.53}$$

$$F^{NO_3} = \frac{(\alpha_{Sul})^2}{((\alpha_{Sul})^2 + [O_2]^2)} \tag{3.54}$$

with $(\alpha_{Sul})^2 = 5 \times 10^{-13}\, mol^2\, kg^{-2}$.

The four maximal conversion rates calculated in Equations 3.48-3.51 are further modified in an iterative numerical method. As a general rule, if one or more reactants are depleted, the available amount of these tracers is distributed over the two possible reactions. A scaling factor f_X is defined for each reactive tracer, i.e. for hydrogen sulfide, oxygen, nitrate and elemental sulfur. This scaling factor then defines the conversion rate at the respective iterative step and the faster reaction receives the greater proportion of the reactant. The consecutive calculations of reaction rates is summerized in Table 3.4. Changes in tracer concentration $\Delta[X]$, the scaling factor f_X for each reactive tracer and the two new conversion rates are given for each step. The final rates $l^{O_2}_{H_2S,S^0}$, $l^{NO_3}_{H_2S,S^0}$, $l^{O_2}_{S^0,SO_4}$ and $l^{NO_3}_{S^0,SO_4}$ are used to update the concentrations of hydrogen sulfide, oxygen, nitrate and elemental sulfur. This iterative scheme is not fully symmetric in all variables and depends on the time step. It should be improved in future model versions.

Tab. 3.4
Iterative calculation of oxidation rates of hydrogen sulfide and elemental sulfur with either oxygen or nitrate. Final conversion rates are highlighted in bold type. S_{12}, s_{13} are the stoichiometric constants of the oxidation with oxygen and s_{14}, s_{15} are the respective constants of the oxidation with nitrate.

Tab. 3.4
Iterative Berechnung der Oxidationsraten von Schwefelwasserstoff und elementarem Schwefel mit entweder Sauerstoff oder Nitrat. Finale Raten sind in fett hervorgehoben. S_{12}, s_{13} sind die stöchiometrischen Konstanten der Oxidation von Schwefelwasserstoff und elementarem Schwefel mit Sauerstoff und s_{14}, s_{15} sind die entsprechenden Konstanten der Oxidation mit Nitrat.

Step	**Changes in tracer concentration per time step**	**Scaling factor**	**Conversion rates**
1	$\Delta[H_2S] = ({}^{(1)}l^{O_2}_{H_2S,S^0} + {}^{(1)}l^{NO_3}_{H_2S,S^0})\,\Delta t$	$f_{H_2S} = \frac{\min(\Delta[H_2S],[H_2S])}{\Delta[H_2S]}$	${}^{(2)}l^{O_2}_{H_2S,S^0} = {}^{(1)}l^{O_2}_{H_2S,S^0}\, f_{H_2S}$
			${}^{(2)}l^{NO_3}_{H_2S,S^0} = {}^{(1)}l^{NO_3}_{H_2S,S^0}\, f_{H_2S}$
2	$\Delta[O_2] = (s_{10}\,{}^{(2)}l^{O_2}_{H_2S,S^0} + s_{11}\,{}^{(1)}l^{O_2}_{S^0,SO_4})\,\Delta t$	$f_{O_2} = \frac{\min(\Delta[O_2],[O_2])}{\Delta[O_2]}$	$\boldsymbol{l^{O_2}_{H_2S,S^0}} = {}^{(2)}l^{O_2}_{H_2S,S^0}\, f_{O_2}$
			${}^{(2)}l^{O_2}_{S^0,SO_4} = {}^{(1)}l^{O_2}_{S^0,SO_4}\, f_{O_2}$
3	$\Delta[NO_3] = (s_{12}\,{}^{(2)}l^{NO_3}_{H_2S,S^0} + s_{13}\,{}^{(1)}l^{NO_3}_{S^0,SO_4})\,\Delta t$	$f_{NO_3} = \frac{\min(\Delta[NO_3],[NO_3])}{\Delta[NO_3]}$	$\boldsymbol{l^{NO_3}_{H_2S,S^0}} = {}^{(2)}l^{NO_3}_{H_2S,S^0}\, f_{NO_3}$
			${}^{(2)}l^{NO_3}_{S^0,SO_4} = {}^{(1)}l^{NO_3}_{S^0,SO_4}\, f_{NO_3}$
4	$\Delta[S] = ({}^{(2)}l^{O_2}_{S^0,SO_4} + {}^{(2)}l^{NO_3}_{S^0,SO_4})\,\Delta t$	$f_S = \frac{\min(\Delta[S],[S]+(l^{O_2}_{H_2S,S^0}+l^{NO_3}_{H_2S,S^0})\,\Delta t)}{\Delta[S]}$	$\boldsymbol{l^{O_2}_{S^0,SO_4}} = {}^{(2)}l^{O_2}_{S^0,SO_4}\, f_S$
			$\boldsymbol{l^{NO_3}_{S^0,SO_4}} = {}^{(2)}l^{NO_3}_{S^0,SO_4}\, f_S$

3.5 Modeled processes in the sediment

The 'Sediment-detritus' is in the same way mineralised by prokaryotes as the sinking 'Detritus' in the water column. Mineralisation of 'Sediment-detritus' takes place by oxygen respiration, denitrification or sulfate reduction. Anammox in the sediment is not considered.

If a certain thickness of the sediment is reached, all sediment below this layer is considered as buried (NEUMANN & SCHERNEWSKI, 2008). Buried detritus and nutrients are not recycled as long as resuspension events eventually diminish the thickness of the sediment layer. Furthermore, the sulfur bacteria distributed on the oxic and hypoxic sediment surface, depend on permanent supply of hydrogen sulfide from below. Hence, their occurrence is coupled to the amount of nitrogen stored in the sediment:

- If less then a certain amount of nitrogen (N_{min}^{Sed}) is stored in the sediment ('thin, partially oxic/anoxic sediments', 3.5.1), the redoxcline is mostly found within the sediment, a permanent release of hydrogen sulfide is unlikely and sulfur bacteria are assumed to be absent. In this case bottom water directly interacts with the sediment and the processes in the sediment depend on the bottom water properties.
- If more than a certain amount of nitrogen (N_{min}^{Sed}) is stored in the sediment ('thick, anoxic sediments', 3.5.2), the redoxcline is permanently at or even above the sediment surface. Hydrogen sulfide released from sulfate reduction sustains mats of sulfur bacteria. These, in turn, prevent the diffusion of oxygen and nitrate from the bottom water into the sediment.

Accordingly, 'available Sediment-Detritus' $[SD]^{avail}$ is defined:

$$[SD]^{avail} = \min\left(N_{min}^{Sed}, [SD]\right), \tag{3.55}$$

with $N_{min}^{Sed} = 1\,mol\,m^{-2}$.

Similar to mineralisation of 'Detritus' in the water column, the mineralisation rate of 'Sediment-detritus' is temperature dependent:

$$l_{SD,NH_3}^{Sed}(T) = k_{SD,NH_3}^{Sed,0}\,F^T, \tag{3.56}$$

$$F^T = e^{\beta_{Sed}\,T}, \tag{3.57}$$

with $k_{SD,NH_3}^{Sed,0} = 0.003\,d^{-1}$ and $\beta_{Sed} = 0.0693\,K^{-1}$ which is equivalent to $Q_{10} = 2$ of the van 't Hoff's rule, i.e. mineralisation rate increases by factor 2 when temperature increases by $10\,K$.

The total amount of 'Sediment-detritus' $[SD]$ mineralised in one time step is:

$$\Delta[SD] = l_{SD,NH_3}^{Sed}\,[SD]^{avail}\,\Delta t. \tag{3.58}$$

Depending on the thickness of the sediment, 'Sediment-detritus' is mineralised by oxygen respiration, denitrification and/or sulfate reduction, but not by Anammox. The different schemes of 'thin, partially oxic/anoxic sediments' and 'thick, anoxic sediments' are described below.

3.5.1 Mineralisation of detritus in thin, partially oxic/anoxic sediments

In thin, partially oxic/anoxic sediments, the redoxcline is mostly found within the sediment and the bottom water is oxic. 'Sediment-detritus' is mineralised stepwise by oxygen respiration,

denitrification and sulfate reduction. Additionally, a permanent surplus mineralisation from denitrification occurs in these sediments ($\Delta[SD]^{Den}_{surp}$). Only if the bottom water over the sediment is anoxic, the total mineralisation rate is initially reduced by the factor f^{Sed}_{anox}:

$$\Delta[SD] = \Delta[SD]\, f^{Sed}_{anox}, \tag{3.59}$$

$$\Delta[SD] = \Delta[SD]^{Oxy} + \Delta[SD]^{Den} + \Delta[SD]^{Sul}, \tag{3.60}$$

with $f^{Sed}_{anox} = 0.3$. $\Delta[SD]$ is derived in Equation 3.58.

The consumed oxygen and the corresponding amount of mineralised 'Sediment-detritus' from oxygen mineralisation are:

$$\Delta[O_2]^{\uparrow} = \min\left([O_2]\, h, s_6\, \Delta[SD]\right), \tag{3.61}$$

$$\Delta[SD]^{Oxy} = \frac{\Delta[O_2]}{s_6}, \tag{3.62}$$

where $[O_2]\, h$ is the amount of oxygen in the bottom-most cell of height h, s_6 is the stoichiometric constant of oxygen respiration.

If oxygen is depleted, heterotrophic denitrification of the remaining sediment takes place. The amount of nitrate used for denitrification is:

$$\Delta[NO_3]^{\uparrow} = \min\left([NO_3]\, h, s_7\left(\Delta[SD] - \Delta[SD]^{Oxy}\right)\right), \tag{3.63}$$

$$\Delta[SD]^{Den} = \frac{\Delta[NO_3]}{s_7}, \tag{3.64}$$

where $[NO_3]\, h$ is the amount of nitrate in the bottom-most cell of height h, s_7 is the stoichiometric constant of heterotrophic denitrification.

In thin, anoxic sediment layers, sulfate-reducing prokaryotes release some hydrogen sulfide that, however, cannot support a permanent mat of sulfur bacteria. Accordingly, hydrogen sulfide is released from the sediment into the bottom water:

$$\Delta[H_2S]^{\uparrow} = s_8\left(\Delta[SD] - \Delta[SD]^{Oxy} - \Delta[SD]^{Den}\right), \tag{3.65}$$

$$\Delta[SD]^{Sul} = \frac{\Delta[H_2S]}{s_8}. \tag{3.66}$$

where s_8 is the stoichiometric constant of heterotrophic sulfate reduction.

Surplus denitrification at the sediment redoxcline. Within thin, oxic sediments, a specific fraction f^{Sed}_{nit} of the ammonium released from mineralisation is directly nitrified to nitrate. The produced nitrate, in turn, is assumed to be consumed immediately and locally by heterotrophic denitrification. Hence, a permanent surplus denitrification occurs in these sediments (Neumann & Schernewski, 2008).

The consumed oxygen for nitrification of ammonium within the sedimenand and the released nitrate by this process are:

$$\Delta[O_2]_{surp} \uparrow = \theta([O_2])\, s_5\, \Delta[NH_3]\, f_{nit}^{Sed}, \tag{3.67}$$

$$\Delta[NO_3]_{surp} \uparrow = \theta([O_2])\, \Delta[NH_3]\, f_{nit}^{Sed}, \tag{3.68}$$

$$\Delta[N_2]_{surp} \uparrow = \frac{1}{2}\, \Delta[NH_3]\, f_{nit}^{Sed}, \tag{3.69}$$

where s_5 is the stoichiometric constant of nitrification linking oxygen and ammonium. The stoichiometric ratio of ammonium and nitrate during nitrification is $1:1$ and consumption of 2 mol nitrate during denitrification yields 1 mol dinitrogen. $\Delta[NH_3]\, f_{nit}^{Sed}$ is the fraction of the ammonium produced by mineralisation and is immediately nitrified to nitrate with $f_{nit}^{Sed} = 0.5$. Nitrification is limited by the available oxygen $\theta([O_2])$.

The additional 'Sediment-detritus' mineralised with surplus nitrate by surplus denitrification $\Delta[SD]_{surp}^{Den}$ is:

$$\Delta[SD]_{surp}^{Den} = \frac{\Delta[NO_3]_{surp}}{s_7}. \tag{3.70}$$

where s_7 is the stoichiometric constant of heterotrophic denitrification.

Surplus denitrification reaction at the sediment redoxcline causes an additional ammonium, phosphate and dinitrogen release. Hence, the total amount of ammonium, phosphate and dinitrogen released from thin, partially oxic/anoxic sediments is:

$$\Delta[NH_3]^{thin} \uparrow = \Delta[SD] + \Delta[SD]_{surp}^{Den} - \theta([O_2])\, \Delta[SD]\, f_{nit}^{Sed}, \tag{3.71}$$

$$\Delta[PO_4]^{thin} \uparrow = s_1 \Delta[NH_3]^{thin}, \tag{3.72}$$

where s_1 is the Redfield phosphorus:nitrogen ratio.

Even though phosphate released from the anoxic sediment to oxic bottom water was found to be scavenged by colloidal iron oxohydroxide (Gunnars & Blomqvist, 1997), phosphate scavenging is expected to be less efficient in the Benguela upwelling sediment where iron availability is generally low. Accordingly, this process is not implemented in the model.

The bottom tracer fluxes, both into the sediment $B_{X,SD}$ and out of the sediment $B_{SD,X}$, at the surface of thin, partially oxic/anoxic sediments can now be derived (Tab. 3.5) and they differ from 'thick anoxic sediments' (see 3.5.2).

Tab. 3.5
Bottom tracer fluxes in thin, partially oxic/anoxic sediments.

Tab. 3.5
Bodenflüsse von Wasserinhaltsstoffen in dünnen, teilweise oxischen/anoxischen Sedimenten.

Tracer	**Bottom tracer fluxes into the sediment** $B_{X,SD}$ **Bottom tracer fluxes out of the sediment** $B_{SD,X}$	
Nitrate	$B_{NO_3,SD} =$	$\min\left([NO_3]\,h,\, s_7(\Delta[SD]^{Den} + \Delta[SD]^{Den}_{surp})\right)$
	$B_{SD,NO_3} =$	0
Ammonium	$B_{NH_3,SD} =$	0
	$B_{SD,NH_3} =$	$\Delta[SD] + \Delta[SD]^{Den}_{surp} - \theta([O_2])\,\Delta[SD]\,f^{Sed}_{nit}$
Phosphate	$B_{PO_4,SD} =$	0
	$B_{SD,PO_4} =$	$s_1 B_{SD,NH_3}$
Oxygen	$B_{O_2,SD} =$	$\min\left([O_2]\,h, s_6\,\Delta[SD]\right) + \theta([O_2])\,s_5\,\Delta[NH_3]\,f^{Sed}_{nit}$
	$B_{SD,O_2} =$	0
Hydrogen sulfide	$B_{H_2S,SD} =$	0
	$B_{SD,H_2S} =$	$s_8\,(\Delta[SD] - \Delta[SD]^{Oxy} - \Delta[SD]^{Den})$

3.5.2 Mineralisation of detritus in thick, anoxic sediments

Thick sediments are always anoxic and nitrate is assumed to be depleted. The total mineralisation rate is initially reduced by the factor f^{Sed}_{anox} and only heterotrophic sulfate reduction of 'Sediment-detritus' takes place within the sediment releasing dissolved hydrogen sulfide into the sediment:

$$\Delta[SD] = \Delta[SD]\,f^{Sed}_{anox}, \tag{3.73}$$

$$\Delta[H_2S] = s_8\,\Delta[SD], \tag{3.74}$$

with $f^{Sed}_{anox} = 0.3$ and s_8 is the stoichiometric constant of heterotrophic sulfate reduction. $\Delta[SD]$ is derived in Equation 3.58.

Sulfur bacteria colonise the upper sediment layer and oxidise hydrogen sulfide, i.e. it is not released to the near bottom water. If available, sulfur-bacteria prefer the energetically more favorable oxidation with oxygen:

$$\Delta[O_2] = \frac{\Delta[H_2S]}{s_{14}} = \frac{s_8}{s_{14}}\Delta[SD]. \tag{3.75}$$

where s_8 is the stoichiometric constant of heterotrophic sulfate reduction and s_{14} is the stoichiometric constant of the oxidation of hydrogen sulfide to sulfate with oxygen in the sediment.

Most likely, the amount of oxygen in the bottom water is not sufficient to oxidise hydrogen sulfide completely. Hence, sulfide oxidation is limited by the oxygen content of the bottom cell:

$$\Delta[O_2] = \min\left([O_2]\,h, \frac{s_8}{s_{14}}\,\Delta[SD]\right), \tag{3.76}$$

$$\Delta[H_2S]^{O_2} = s_{14}\,\Delta[O_2], \tag{3.77}$$

where $[O_2]\,h$ is the amount of oxygen in the bottom-most cell of height h. $\Delta[H_2S]^{O_2}$ is the amount of hydrogen sulfide oxidised with oxygen.

If the bottom water is anoxic, but nitrate is present, sulfur bacteria oxidise hydrogen sulfide with nitrate through the process of DNRA (dissimilatory naitrate reduction to ammonium), see 2.3.10.

$$\Delta[NO_3] = \min\left([NO_3]\,h, s_{15}\left(\Delta[H_2S] - \Delta[H_2S]^{O_2}\right)\right), \tag{3.78}$$

$$\Delta[H_2S]^{NO_3} = s_{15}\,\Delta[NO_3] \tag{3.79}$$

where $[NO_3]\,h$ is the amount of nitrate in the bottom-most cell of height h and s_{15} is the stoichiometric constant of the oxidation of hydrogen sulfide to sulfate with nitrate in the sediment.

Only if the the amount of oxygen and nitrate in the bottom water is not sufficient to oxidise the hydrogen sulfide completely, free hydrogen sulfide is released into the water column:

$$\Delta[H_2S]^{\uparrow} = (\Delta[H_2S] - \Delta[H_2S]^{O_2} - \Delta[H_2S]^{NO_3}). \tag{3.80}$$

$$\tag{3.81}$$

The process of DNRA causes an additional ammonium release. Hence, the total amount of ammonium and phosphate released from thick, anoxic sediments is:

$$\Delta[NH_3]^{thick}\uparrow = \Delta[SD] + \Delta[NO_3], \tag{3.82}$$

$$\Delta[PO_4]^{thick}\uparrow = s_1\Delta[SD], \tag{3.83}$$

where s_1 is the Redfield phosphorus:nitrogen ratio. The stoichiometric ratio of nitrate and ammonium during DNRA is $1:1$.

The bottom tracer fluxes, both into the sediment $B_{X,SD}$ and out of the sediment $B_{SD,X}$, at the surface of 'thick, anoxic sediments' can now be derived (Tab. 3.6) and differ from 'thin, partially oxic/anoxic sediments' (see 3.5.1).

Tab. 3.6
Bottom tracer fluxes in thick, anoxic sediments.

Tab. 3.6
Bodenflüsse von Wasserinhaltsstoffen in dicken, anoxischen Sedimenten.

Tracer	**Bottom tracer fluxes into the sediment $B_{X,SD}$** **Bottom tracer fluxes out of the sediment $B_{SD,X}$**
Nitrate	$B_{NO_3,SD} = \min\left([NO_3]\, h, s_{15}(\Delta[SD] - \Delta[SD]^{Oxy})\right)$
	$B_{SD,NO_3} = 0$
Ammonium	$B_{NH_3,SD} = 0$
	$B_{SD,NH_3} = l^{Sed}_{SD,NH_3}[SD]^{avail} + B_{NO_3,SD}$
Phosphate	$B_{PO_4,SD} = 0$
	$B_{SD,PO_4} = s_1 B_{SD,NH_3}$
Oxygen	$B_{O_2,SD} = \min\left([O_2]\, h\,, s_{14}(\Delta[SD])\right)$
	$B_{SD,O_2} = 0$
Hydrogen sulfide	$B_{H_2S,SD} = 0$
	$B_{SD,H_2S} = \left([s_8 \Delta SD] - s_{14}\Delta[O_2] - s_{15}\Delta[NO_3]\right)$

3.6 Parameters of the ecosystem model

Tab. 3.7
Parameters of the ecosystem model: Three phytoplankton functional types, referred to as 'Diatoms', 'Flagellates' and 'Cyanobacteria'.

Tab. 3.7
Parameter des Ökosystemmodells: Drei funktionelle Phytoplanktontypen, bezeichnet als 'Diatomeen', 'Flagellate' und 'Cyanobakterien'.

Parameter	**Symbol**	**'Diatoms'**	**'Flagellates'**	**'Cyanobacteria'**	**Unit**
Maximal specific growth rates	r_0	1.5	0.8	0.6	d^{-1}
Natural maximal specific mortality rates	$l_{P,D}$	0.02	0.02	0.02	d^{-1}
Maximal specific respiration rates	l_{P,NH_3}	0.01	0.01	0.01	d^{-1}
Half-saturation constant of nutrient uptake	α	6.00×10^{-6}	1.80×10^{-6}	2.25×10^{-6}	$mol\,kg^{-1}$
Minimum PAR acclimation	I_{min}	25	50	50	$W\,m^{-2}$
Minimum growth temperature	T_{min}	not defined	not defined	20	$°C$
Sinking rates	w_P^{sink}	-1	not defined	not defined	$m\,d^{-1}$

Tab. 3.8
Parameters of the ecosystem model: Three zooplankton functional types, referred to as 'Copepodes', 'Krill 1' and 'Krill 2'.

Tab. 3.8
Parameter des Ökosystemmodells: Drei funktionelle Zooplanktontypen, bezeichnet als 'Copepoden', 'Krill 1' und 'Krill 2'.

Parameter	**Symbol**	**'Copepodes'**	**'Krill 1'**	**'Krill 2'**	**Unit**
Maximal specific grazing rates	g_0	1.0	0.5	0.5	d^{-1}
Natural maximal mortality rates	$l_{Z,D}^{nat}$	0.03	0.01	0.01	d^{-1}
Maximal respiration rates	l_{Z,NH_3}^{resp}	0.03	0.01	0.01	d^{-1}
Closure term of the model (part of the zooplankton mortality)	z^{clos}	6.67×10^5			$kg\,mol{-}1$
Optimal temperature of grazing	T_{opt}	15	15	10	$°C$
Maximal temperature of grazing	T_{max}	25	25	15	$°C$
Shape parameter for temperature dependence of grazing	β	1.7	1.7	1.7	dimensionless
$Ivlev$ parameter of zooplankton grazing	Iv	1.0×10^6	1.0×10^6	1.0×10^6	$kg\,mol^{-1}$
Excretion of ammonium by sloppy feeding	a_{ex,NH_3}	0.18	0.18	0.18	dimensionless
Excretion of detritus by sloppy feeding	$a_{ex,D}$	0.18	0.18	0.18	dimensionless
Sinking velocity	$w_Z^{sink,0}$	not defined	-800	-600	$m\,d^{-1}$
Velocity of upward movement	$w_Z^{rise,0}$	not defined	1600	1200	$m\,d^{-1}$
Maximal PAR where zooplankton upward movement stops	I_{max}	not defined	1.0×10^{-20}	1.0×10^{-10}	$mol\,photons\,m^{-2}\,s^{-1}$
Minimum dissolved oxygen concentration where zooplankton sinking stops	O_2^{min}	not defined	5.0×10^{-6}	5.0×10^{-6}	$mol\,kg^{-1}$
Maximum hydrogen sulfide concentration where zooplankton sinking stops	H_2S^{max}	not defined	1.0×10^{-6}	1.0×10^{-6}	$mol\,kg^{-1}$

Tab. 3.9
Parameters of the ecosystem model: detritus and microbial processes.

Tab. 3.9
Parameter des Ökosystemmodells: Detritus und mikrobielle Prozesse.

Parameter		**Symbol**	**Value**	**Unit**
Detritus sinking rate	Water column	w_D^{sink}	-3	$m\,d^{-1}$
Maximal nitrification rate	Water column	k_{Nit}^0	0.03	d^{-1}
Temperature dependence of nitrification	Water column	β_{Nit}	0.11	$K{-}1$
Half-saturation constant of the oxygen-dependence of nitrification	Water column	α_{Nit}	3.75×10^{-6}	$mol\,kg^{-1}$
Total mineralisation rate of detritus	Water column	k_{D,NH_3}^0	0.003	d^{-1}
Temperature dependence of mineralisation of detritus	Water column	β_{min}	0.0693	K^{-1}
Maximal anammox rate	Water column	k_{Ana}^0	0.02	d^{-1}
Smooth oxygen switch for detritus recycling	Water column	α_{O_2}	5.0×10^5	$kg\,mol^{-1}$
Smooth nitrate switch for detritus recycling	Water column	α_{NO_3}	2.2×10^6	$kg\,mol^{-1}$
Smooth hydrogen sulfide switch for detritus recycling	Water column	α_{H_2S}	5.0×10^3	$kg\,mol^{-1}$
Smooth ammonium switch for detritus recycling	Water column	α_{NH_3}	2.2×10^6	$kg\,mol^{-1}$
Hydrogen sulfide oxidation rate with oxygen	Water column	$k_{H_2S,S^0}^{O_2,0}$	8×10^5	d^{-1}
Hydrogen sulfide oxidation rate with nitrate	Water column	$k_{H_2S,S^0}^{NO_3,0}$	8×10^5	d^{-1}
Elemental sulfur oxidation rate with oxygen	Water column	$k_{S^0,SO_4}^{O_2,0}$	2×10^3	d^{-1}
Elemental sulfur oxidation rate with nitrate	Water column	$k_{S^0,SO_4}^{NO_3,0}$	2×10^3	d^{-1}
Temperature dependence of sulfide and sulfur oxidation	Water column	β_{Sul}	0.0693	K^{-1}
Oxygen over nitrate preference for sulfide and sulfur oxidation	Water column	$(\alpha_{Sul})^2$	5×10^{-13}	$mol^2\,kg^{-2}$
Minimum nitrogen content of active sediment to support growth of sulfur bacteria	Sediment	N_{min}^{Sed}	1.0	$mol\,m^{-2}$
Maximal mineralisation rate of sediment-detritus	Sediment	$k_{SD,NH_3}^{Sed,0}$	0.003	d^{-1}
Temperature dependence of mineralisation of sediment-detritus	Sediment	β_{Sed}	0.0693	K^{-1}
Fraction of mineralisation in thin sediments for anoxic bottom water	Sediment	f_{anox}^{Sed}	0.3	dimensionless
Fraction of denitrification at the sediment redoxcline	Sediment	f_{nit}^{Sed}	0.5	dimensionless

4 The physical model component

4.1 The basic physical equations

The physical model component for the calculation of currents and the advection and diffusion of tracers is *MOM-4*. A detailed documentation of this circulation model is given in the manual, many methods are described in GRIFFIES (2004). The model version used here exploits an explicit free surface scheme for the sea level elevation and fresh water flux (GRIFFIES ET AL., 2001). The *MOM-4* code solves the so called primitive equations in Boussinesque approximation. Vertical velocity is diagnosed from the condition of non-divergent flow, pressure is calculated in hydrostatic approximation. The momentum equations are supplemented by advection-diffusion equations for salinity and heat (temperature). The density is calculated according to the revised seawater equation of state from temperature, salinity and pressure (JACKETT ET AL., 2006). The set of prognostic model variables comprises sea level, the horizontal velocity, $\mathbf{u}$, the active tracers temperature T and salinity, S. The vertical velocity w is diagnosed from the divergency of the horizontal velocity field. Ecosystem variables like nutrients and planktonic organisms are represented like tracer variables.

Turbulence is not treated explicitly but enters the equations as Reynolds stress, i.e. as vertical and horizontal turbulent viscosity and mixing. *MOM-4* offers several alternatives to calculate these quantities. The choice of parameterisations used for this model setup will be described in section 4.3.1 and 4.3.3.

4.2 Spatial differencing and time stepping

An ARAKAWA B-grid is used in *MOM-4*. Spatial derivatives are central differences, time stepping is a staggert Euler foreward scheme with time step $\Delta\tau$, i.e., tracer variables are updated from a time level τ to $\tau+\Delta t$, the horizontal velocity, $\mathbf{u}$, is updated from $\tau-\Delta\tau/2$ to $\tau+\Delta\tau/2$, whereby advective fluxes and forces are calculated from variables at time level $\tau+\Delta\tau/2$. To find the grid cell height for tracers and velocities the sea level is needed at both, integer and half-integer time steps. The sea level η^b is updated together with the vertically integrated velocity with a much smaller time step, Δt. To ensure tracer conservation, another variable representing the sea level, $\eta(\tau)$, is updated with the same numerical scheme like the tracer variables. This requires a special coupling between the barotropic and the baroclinic mode as described in Appendix A. The varying height of the surface cells is taken into account, the optional $z^\star$-coordinates (STACEY ET AL., 1995) are used distributing the undulations of the sea surface vertically over all grid cells.

The baroclinic equations are updated to time level $\tau+\Delta\tau/2$, using a time step governed by the baroclinic wave speed and by viscosity. To allow for a larger time-step, barotropic velocity components are removed from the total velocity by vertical averaging. A detailed description how the mode splitting is implemented under the special consideration of tracer conservation is given in Appendix A as well as in GRIFFIES ET AL. (2001) and GRIFFIES (2004).

4.3 Turbulent closure

4.3.1 Vertical viscosity and mixing

The nonlocal K-profile model is invoked for turbulent vertical processes (LARGE ET AL., 1994). This scheme delivers not only vertical mixing and viscosity coefficients but also a boundary layer depth h, which is used in the ecosystem model. The results for the surface boundary layer depth h reveal as sensitive to the choice of the model parameters. In the current experiments, the parameters for the determination of h are not changed from the original values.

Below the surface boundary layer, mixing and viscosity come from shear induced turbulence and from breaking of internal waves,

$$\nu_{t,m} = \nu^w_{t,m} + \nu^s_{t,m}. \tag{4.1}$$

Internal wave breaking is represented by a mixing coefficient, ν^w_t and viscosity coefficients ν^w_m,

$$\nu^w_t = 10^{-6} \quad .. \quad 10^{-5}\, m^2\, s^{-1} \tag{4.2}$$
$$\nu^w_m = 10^{-5} \quad .. \quad 10^{-4}\, m^2\, s^{-1}. \tag{4.3}$$

Modifications to the standard scheme are described in section 4.3.2. Shear induced mixing is parameterized in terms of a local gradient Richardson number,

$$R_g = \frac{N^2}{(\partial_z U)^2 + (\partial_z V)^2}. \tag{4.4}$$

Two versions are used. One is the scheme of Peters (PETERS ET AL., 1988):

$$\nu^s_{t,m} = \nu^0_{t,m} \qquad R_g < 0, \tag{4.5}$$
$$\nu^s_{t,m} = \nu^0_{t,m} \left(1 - \left(\frac{R_g}{R_0}\right)^2\right)^3 \qquad 0 < R_g < R_0, \tag{4.6}$$
$$\nu^s_{t,m} = 0 \qquad R_g > R_0, \tag{4.7}$$

The parameters are $R_0 = 0.7$ and

$$\nu^0_t = 1 \times 10^{-3} \quad .. \quad 5 \times 10^{-3}\, m^2\, s^{-1},$$
$$\nu^0_m = 1 \times 10^{-3} \quad .. \quad 1 \times 10^{-2}\, m^2\, s^{-1}.$$

The other scheme is described by PACANOWSKI & PHILANDER (1981),

$$\nu^s_t = \nu^0_t \qquad R_g < 0, \tag{4.8}$$
$$\nu^s_t = \nu^0_t \left(1 + \frac{R_g}{2}\right)^3 \qquad R_g > 0, \tag{4.9}$$
$$\nu^s_m = \nu^0_m \left(1 + \frac{R_g}{2}\right)^2 \qquad R_g > 0. \tag{4.10}$$

It depends on the application, which parameterisation is more appropriate.

The mixing coefficient within the boundary layer has the general form

$$K_t(z) = h\, w(z)\, G(z). \tag{4.11}$$

The scale function w is calculated from the Monin-Obukhov similarity theory. It is proportionally to the friction velocity u^*. The dimensionless "shape function" G is adjusted by a matching condition for the diffusivity and its vertical derivative at the bottom of the boundary layer, which allows for boundary layer diffusion driven by turbulence below the boundary layer itself. For all details see LARGE ET AL. (1994).

If the surface boundary layer becomes instable, e.g. by nightly cooling, shear induced mixing is set to very large values in the unstable levels. Because of the matching condition for G, mixing and viscosity in the surface boundary layer becomes generally large which leads to very small vertical tracer gradients. Hence, the calculated down-gradient tracer fluxes may be unrealistically small in the convective limit. To improve this, the total turbulent vertical flux of a quantity x is supplemented with an additional term, which accounts for turbulent transports through the whole boundary layer in the absence of vertical tracer gradients,

$$\overline{wx} = K_x(z)\left(\partial z X - \gamma_x\right). \tag{4.12}$$

The quantity

$$\gamma_x(z) \sim \frac{\overline{wx}_0}{w(z)h} \tag{4.13}$$

acts in the case of convection only and redistributes the tracer surface flux $\overline{wx}_0$ over the surface boundary layer. This term is especially important for convective mixing during nighttime.

The *kpp*-vertical mixing scheme includes diagnostics of the mixing and the mixed layer depth. Some modifications to the original *kpp*-scheme are needed to avoid a failure of the original scheme. In addition, the parameter of the nonlocal vertical mixing is limited, $\gamma_x < 1$, to avoid unrealistic growing vertical tracer gradients. Also the implementation of short wave radiation in *MOM-4* does not follow the scheme proposed in LARGE ET AL. (1994), equation (A.4). In the case of convection during daytime, this scheme counts downward propagation of heat from radiation twice. Such events are usually rare, but it leads occasionally to unrealistically low sea surface temperatures. In the current experiments, the code for heat was corrected as

$$\gamma_x(z) \sim \frac{\overline{w\theta}_0 + \overline{w\theta}_R}{w(z)h}, \tag{4.14}$$

$$\overline{w\theta}_R = I(0) - I(z), \tag{4.15}$$

where $I(z)$ is the power of short wave radiation penetrating into the ocean at depth z.

4.3.2 Modified vertical mixing by internal wave breaking

Experiments with the ecosystem model reveal, that mixing on the shelf is apparently too small to allow enough vertical oxygen diffusion into the bottom water. Hence, enhanced vertical mixing at locations with elevated vertical velocity as at the shelf edge may improve the ecosystem model results. Enhanced mixing near steep topography is introduced as follows:

$$\nu_t^{w,topo} = \left(\nu_{t,bg}^{w,topo} + \nu_{t,0}^{w,topo}\frac{\overline{\Delta H}^p}{H}\right) e^{\frac{z-H}{v_s}}. \tag{4.16}$$

ν is defined at tracer points, the bar refers to the geometric mean of the differences in the height of the adjacent velocity points.

```
delta_h = 0.25*sqrt((hup(i  ,jrow)  - hup(i,  jrow-1))**2 &
                  +  (hup(i-1,jrow)  - hup(i-1,jrow-1))**2 &
                  +  (hup(i,  jrow)  - hup(i-1,jrow  ))**2 &
                  +  (hup(i,  jrow-1)- hup(i-1,jrow-1))**2)
```

The vertical scale function v_s is typically 20 m and limits the enhanced mixing to a bottom layer.

In addition to this local mixing, the constant but horizontally and vertically varying Bryan-Lewis background diffusivity (Bryan & Lewis, 1979) may be used. In this case the resulting total vertical mixing coefficient is

$$\nu_t^w = \nu_t^{w,topo} + \nu_t^{w,BL}. \tag{4.17}$$

Other background mixing in the kpp-module is set to zero.

4.3.3 Horizontal viscosity and mixing

The model implementation is "eddy resolving" in the region of interest. Hence, the turbulent terms are needed more for numerical stability of the advection scheme than for the parameterisation of unresolved transport processes. The Smagorinski scheme (Smagorinsky, 1963) is used for horizontal viscosity. The viscosity coefficients are proportionally to a parameter k_{smag}, they scale with the square of the grid spacing and are growing with stress and strain of the velocity field. If stress and strain are small a "background" value

$$A_m^{back} = \frac{2 v_{micom} \Delta x \, \Delta y}{\Delta x + \Delta y}, \tag{4.18}$$

applies. The following parameters are used, $k_{smag_iso} = 2.0$, $v_{micom} = 1 \cdot 10^{-3} \mathrm{m\,s^{-1}}$. Optionally, enhanced resolution dependent background viscosity of the form

$$A_m^{back} = \frac{2 v_{micom} \Delta x \, \Delta y}{\Delta x + \Delta y} \, e^{\frac{-z}{v_s}} \tag{4.19}$$

can be applied. Also negative values for v_s are possible, which can be used to control deep unrealistic currents near open boundaries.

4.4 Control of tracer advection

For tracer advection, positive schemes are available in *MOM-4*, mostly the "mdfl-sweby"-scheme (Hundsdorfer & Trompert, 1994) is used. It turns out, that horizontal tracer diffusion can be chosen as very small. Doing so, sometimes spurious negative values of ecosystem variables are found especially when its concentration is generally small. A simple dependable solution for this problem is to replace negative concentrations by zero in the calculation of tracer time tendencies. It has been proven, that this does not violate tracer conservation and resolves the problem.

4.5 Implementation of open boundary conditions

The application of open boundary conditions for the explicit free surface scheme in *MOM-4*, as used here, is described in detail in Herzfeld et al. (2011). The model boundary is

implemented for the Arakawa B-grid and is placed at tracer points. The boundary condition for the sea level has two major components, a radiation condition using a diagnosed phase velocity and relaxation towards prescribed data. Similarly, tracer equations are closed by a radiation condition in combination with upstream tracer advection and relaxation towards prescribed data.

4.5.1 The radiation condition for the sea level

The diagnostics of a phase velocity for barotropic waves requires measures to remove numerical noise. The scheme involves the following steps, which is repeated each baroclinic time step:

- An initial value from the time averaged sea level η is diagnosed. For outgoing waves, a minimum and maximum value may be enforced. For incoming waves, the phase speed is set to zero. No OBC-data must be stored with this initial value for a model restart.
- For each barotropic time step, a value for the phase speed is diagnosed from the actual sea level η^b. As this value reveals as highly fluctuating, a running time mean smoother is applied. The sea level at the boundary is updated implicitly with this radiation condition.
- If a sequence of barotropic time steps is ready, the sea level η is updated again with a Euler time step. At the open boundary this is done using the final smoothed phase speed for the time tendency.

4.5.2 Relaxation of the sea level towards prescribed data

The rate of relaxation of the sea level towards prescribed values depends on the diagnosed phase velocity. For incoming waves rapid relaxation applies, for outgoing waves relaxation is slower. To avoid numerical oscillations, both the "incoming" and the "outgoing" value of the relaxation coefficient are blended linearly. Relaxation is applied implicitly.

4.5.3 Consideration of the along boundary velocity

At boundary points, the convergence of the barotropic flow is replaced by the cross boundary phase velocity. However, if boundary points have a coast to the right in the southern hemisphere, incoming waves cannot propagate in-ward along the coastline. This results in a clamped sea level, and strong localised unrealistic currents may grow near such points. If the convergence of the along-boundary currents is taken into account for the sea level time tendency, the artificial flow patterns mostly disappear. This option is used in the regional Atlantic model.

4.5.4 Advection and diffusion of tracers

Advection velocity u_B at the inner and outer face of boundary tracer cells is considered as constant. With this assumption a simple upstream approximation for tracer advection is implemented here for a western boundary,

$$ADV = -u_B \begin{cases} T_{B-1} - T_B & : \text{ outgoing} \\ T_B - T^{data} & : \text{ incoming} \end{cases} \tag{4.20}$$

where T^{data} is the prescribed tracer concentration entering the model domain in the case of inflow, T_{B-1} is the tracer at the first internal model point. Vertical diffusion is calculated from

the regular scheme. Horizontal diffusion needs extrapolation beyond the boundary to define all model points involved in the diffusion scheme. This is done by a no-gradient condition,

$$T_{B+1} = T_B. \tag{4.21}$$

Source terms as radiative heat forcing and surface tracer fluxes are applied to avoid gradients between boundary and internal points. At some points near the boundary horizontal mixing can be enhanced. This helps to smooth numerical artifacts and reduces artificial rim current along a boundary.

4.5.5 The radiation condition for tracers

The phase speed at a western boundary is calculated as follows:

$$c^{clin} = -\frac{T_{B-1}(\tau+1) - T_{B-1}(\tau-1)}{T_{B-2}(\tau) - T_{B-1}(\tau)} \frac{\Delta x}{\Delta t}. \tag{4.22}$$

If the sign is positive, waves are incoming and the phase velocity is set to zero, large negative values are clipped with the maximum value allowed for numerical stability. The radiation condition is applied implicitly.

4.5.6 Relaxation of tracers towards prescribed data

The rate of relaxation of the sea level towards prescribed data, R^{clin} depends on the diagnosed phase velocity. If if the sum of phase speed and advection velocity is directed inward, rapid relaxation applies, for outward flow relaxation is slow. For stability the relaxation is carried out implicitly, after all other contributions of the tracer time tendency are applied.

$$T_B(\tau+1) := \frac{T_B(\tau+1) + 2\Delta t\, R^{clin}\, T^{data}}{1 + 2\Delta t\, R^{clin}}. \tag{4.23}$$

4.5.7 Velocity at boundary points

Pressure gradients and Coriolis force as well as surface forces are well defined at boundary points. The friction operator is completed by a no-gradient boundary condition. Enhanced friction near the boundary helps to limit or remove artificial currents near the boundary. Especially unrealistically strong deep currents in the equatorial area can be controlled, if enhanced horizontal background friction of the form 4.19 is applied with a negative scale v_s. The resolution is small in the centre of the model and the background viscosity plays a minor role. Near the boundary the model grid is coarse and viscosity can be enhanced further using features of the OBC-code.

Velocity equations are linearised and horizontal and vertical advection are not considered. Only the metric advection term is taken into account.

4.5.8 A remark about air pressure at the boundary

Inclusion of atmosphere pressure gradients to the surface forcing is often considered as a marginal issue and minor correction because the sea level elevation rapidly adjusts to the air pressure. Slowly varying air pressure gradients are compensated by sea level elevations of the opposite sign and geostropic currents balanced by surface pressure gradients should not be very different with and without air pressure. However, a sea level elevation prescribed at the open boundaries

acts like a reference a reference level. It must be consistent with the atmospheric pressure and the corresponding sea level landscape.

The model described here covers parts of the St.-Helena high pressure area, whose persistent pressure gradients are responsible for the permanent trade winds off Namibia. The boundary data from the large scale model do not consider air pressure, but *MOM-4* does. This inconsistency may lead to strong sea level undulations near the open boundaries in correspondence to unrealistically large amplitudes of deep currents. For this reason, the regional model was run without considering the contribution of air pressure to the surface forcing.

5 Description of the model setup

5.1 The model grid

The model grid resolution is a compromise between requirements of ocean dynamics for resolution and available computer capacity.

The model grid is a rectangular grid in geophysical coordinates (Fig. 5.1). The grid resolution is enhanced in the coastal area off Namibia. The minimum meridional and zonal grid cell size is about 8 km here. The grid is stretched toward the model boundaries. The maximum zonal grid cell size is 17 km near the western boundary, the maximum meridional grid cell size is 18.5 km near the northern boundary and 15 km in the south.

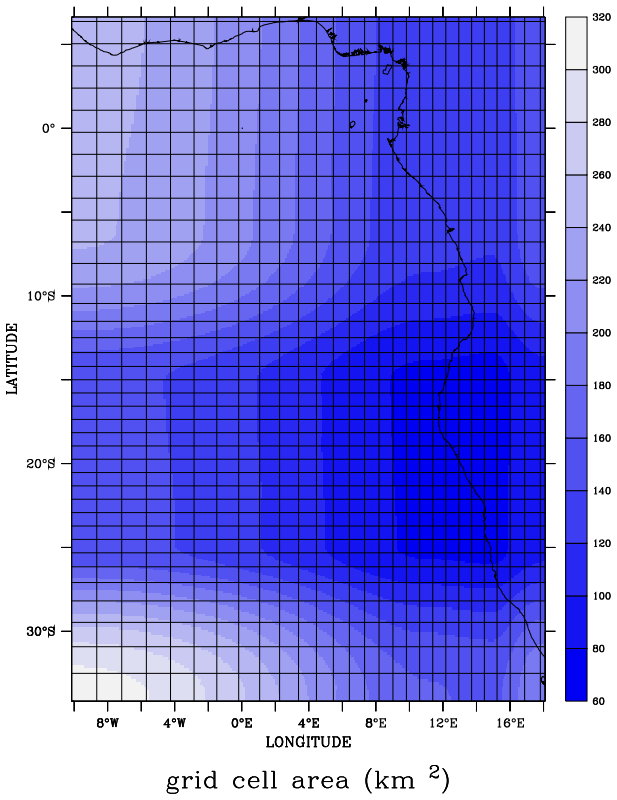

Fig. 5.1
The model grid. The color encodes the typical grid cell area in km^2, only every tenth grid-line is shown.

Abb. 5.1
Das Modellgitter. Die Farbe kodiert die Fläche einer Gitterzelle in km^2, nur jede zehnte Gitterreihe wird gezeigt.

The baroclinic Rossby radius in the model area is resolved with this resolution EMERY ET AL. (1984). However, in shallow waters, especially near the shelf, the Rossby radius is much smaller and the model resolution is not sufficient to allow for all details of coastal processes as upwelling, coastal jets and baroclinic coastal trapped waves.

The vertical grid resolution from the surface to about 200 m depth is constantly at 3 m. Below 120 m, the grid spacing increases like a cosine shaped function to 500 m cell thickness in 5000 m depth. Hence, highest resolution is in the upper model layer and on the shelf. The model grid has been generated with the off-line tools of *MOM-4* PACANOWSKI & GRIFFIES (2000).

5.2 The model topography

The model topography was derived from the *ETOPO-5* (Earth Topography 5-minute), which is a gridded elevation (land) and bathymetry (sea floor) data set for the entire Earth at a grid spacing of 5 minutes (NOAA (1988)). A higher resolved version of *ETOPO-2* exhibits structures at the Namibian shelf which cannot be seen in nautical maps. Hence, the smoother 5 nm topography has been used.

At first, the ocean depth was mapped to the model grid by means of the bilinear regridding methods provided by the Data Visualization and Analysis software *Ferret*. This raw topography was processed with the off-line subroutine *topog* of *MOM-4*. Isolated cells have been filled but without changing the land mask. Shallow areas were deepened to a minimum depth of two grid cells. Partial cells are used, hence topography in deep areas is represented with better resolution than the maximum cell thickness given by the vertical model grid. The maximum depth is limited to 5000 m, a few deeper basins in the model area are restricted to this depth.

This processing was done automatically. The resulting coastline was compared with the coastline provided by WESSEL & SMITH (1996). A few points were manually changed to land or set to minimum ocean depth by hand. Comparing transparent contour plots of the model topography in the Namibian shelf area with nautical maps revealed a sufficient accuracy of the model topography (Fig. 5.2).

The model area contains a couple of rivers which have a great influence on surface water properties even far of the coast. The most prominent in the southern hemisphere is the Congo river with an outflow of up to more than $50000\,m^3\,s^{-1}$. Data on mass transports and river positions have be obtained from the server *aquarius1.gsfc.nasa.gov* and are referenced there to Goddard Space Flight Center. Details on the data source could not be found. For simplicity, all available river discharge data were used even if the amount of fresh water is negligible. The discharge is given as a monthly climatology. The following rivers are considered:
Agneby, Ankobra, Aensu, Bandama, Bengo , Cavally, Cestos, Comoe, Congo, Cross, Cuanza, Foulakari, Kouilou, Kunene, Lobe, Lokoundje, Mono, Niger, Ntem, Nyanga, Nyong, Ogooue, Oranje, Oueme, Pra, Saint John, Sanaga, Sassandra, Sehnkwehn, Sio, Tano, Volta, Wouri.

The river description file suitable for *MOM-4* was generated. Some river locations did not match the river mouth. Depending on the topography, either the river position was moved to a coastal point or some land point was changed to an ocean point of minimum ocean depth.

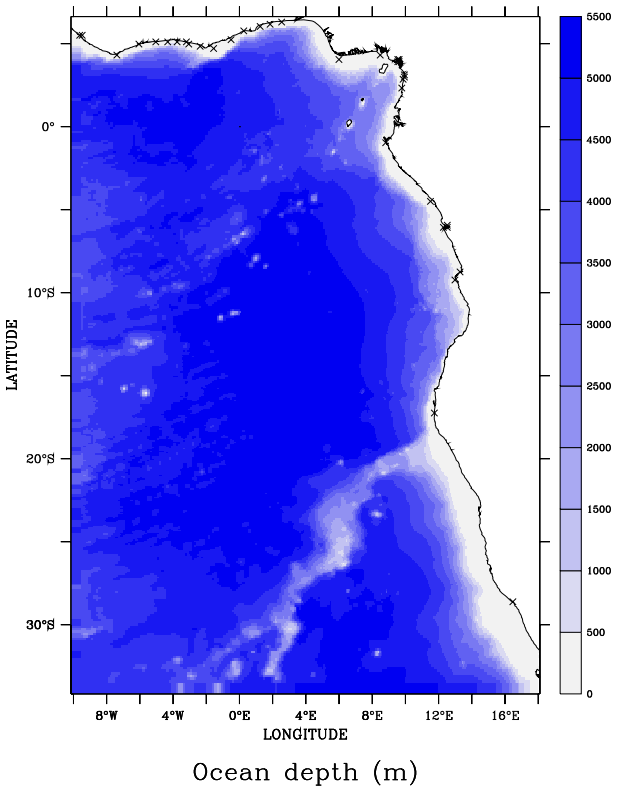

Fig. 5.2
The model topography based on *ETOPO-5*. The crosses mark the position of rivers.

Abb. 5.2
Die Topographie des Modells, die auf *ETOPO-5*-Daten basiert. Die Kreuze kennzeichnen die Lage von Flussmündungen.

The model boundary conditions for a free surface code require the specification of temperature and salinity for the river discharge. Salinity was set to zero. River temperature data were not available. Hence, monthly climatological surface air temperature was used instead and should be a sufficient approximation for the river temperature.

5.3 Boundary data for open boundary conditions

The model grid is an ARAKAWA B-grid and the numerical scheme is complete, if sea level and tracer concentration at the boundaries are prescribed. Hence, only boundary values for these quantities were needed. The *ECCO* consortium (*Estimating the Circulation and Climate of the Ocean*) runs the *MIT* general circulation model. The *ECCO* model results from run *kf080* are chosen as boundary values to drive the regional model. The data set is available on the server *http://ecco.jpl.nasa.gov/datasets/*. Currently the model run is kept updated until the present. The model is defined on a global scale with 1 degree grid spacing and enhanced resolution near the equator. It is driven by *NCEP* reanalysis data that is a product from the National Centers for Environmental Prediction of NOAA. The numerical scheme of the *MIT* model is similar to the used model configuration of *MOM-4*.

Sea level and tracer values (temperature, salinity) have been extracted from the *ECCO* model results from the grid points next to the open boundaries. For the sea level data are given every 12 hours, for temperature and salinity 10 day averages are available. The bilinear regridding methods of the Data Visualization and Analysis software *Ferret* are used to map data from the grid of the *ECCO* model to the regional grid. Differences in the topography of both models are corrected by blanking or downward extrapolation respectively. The experiments described subsequently show, that imbalances in the total transports through the boundaries which are introduced by the interpolation are obviously adjusted by the numerical scheme used at the open boundaries.

It is important, that the *MIT*-model did not consider the air pressure explicitly. First experiments showed strong artificial currents near open boundaries, where sea level data taken from the *ECCO* model are prescribed. The origin of such patterns is a mismatch between the sea level calculated by *MOM-4* under consideration of the air pressure and the boundary data, where information on the air pressure especially on the permanent St.-Helena high pressure area is missing. Disabling air pressure in *MOM-4* resolves the problem and gives smoother results near the open model boundaries.

5.4 Model initialisation

5.4.1 Sea level, currents, temperature and salinity

The model was initialised for sea level, currents, temperature and salinity from a snapshot of the global model of the *ECCO* group gained from *http://ecco.jpl.nasa.gov/datasets*. This ensures initial consistency with the western and southern boundary conditions. Also, sea level, density distribution and currents are already balanced and the regional model benefits to some extend from the model spin up done for the *ECCO* model. Differences in the bottom topography should play a minor role since currents near the bottom are very small.

The output from the *ECCO* model is mapped to the model grid with the bilinear regridding methods of the Data Visualization and Analysis software *Ferret*. Some coastal points, which are land points in the *ECCO* model are filled by extrapolation.

5.4.2 Chemical, biological and sediment variables

Nutrients and oxygen were initialised using data from World Ocean Atlas 2001, Conkright et al. (2002). Monthly climatological data available for the upper 500 m for nitrate and phosphate concentration and for the upper 1500 m for oxygen concentration were combined with the time averaged data for the deep ocean and mapped onto the model grid. Ammonium occurs only at hypoxic or anoxic conditions and was initialised with zero.

Comparing with nutrient data available from field campaigns, the World Ocean Atlas data do not resolve any details of the nutrient and oxygen concentration on the shelf. Hence, these features must be adjusted by the internal model dynamics.

Phytoplankton variables, zooplankton and detritus were initialised only with a minimum value and the development of these variables is left to the model. Sediment was initialised with a constant value, so heterogeneous sediment distribution develops from the model dynamics.

6 Atmospheric forcing

6.1 Data sources

The regional model needs the following fluxes as surface boundary conditions:

- zonal and meridional wind stress
- insolation
- latent and sensible heat flux
- the thermal radiation budget
- the fresh water flux.

These fluxes are derived from the atmosphere variables:

- zonal and meridional wind in 10 m height
- the air pressure at sea level
- the air temperature in 2 m height
- specific humidity in 2 m height
- the cloud coverage
- precipitation

Several data sets are used:

- NCEP reanalysis data. The NCEP data have a spatial resolution of 1.875° and are provided for every 6 hours.
- Spatially and temporally highly resolving results from the regional atmosphere Model REMO.
- Scatterometer wind fields (QuikScat, ASCAT). QuikScat data have a spatial resolution of 0.25° but are provided daily as a composite made from a three day period.
- A combined data set from both NCEP and QuikScat data, whereby the QuikScat wind speed data are modulated with the diurnal cycle extracted from the NCEP data.

6.2 Ocean-atmosphere coupling

6.2.1 Numerical scheme

Ocean and atmosphere are coupled by a boundary layer model. Bulk formulas are used to derive the ocean-atmosphere fluxes from ocean and atmosphere state variables. The fluxes are calculated explicitly, no restoring of sea surface temperature or salinity is used.

The atmosphere model itself is replaced by reading of files with atmosphere data. Hence, any feedback of the ocean to the atmosphere is neglected. The NCEP- and QuikScat atmosphere data can be considered as "realistic" representation of nature. As long as the ocean model does not drift into a completely unrealistic state, this one-way coupling should help to keep the sea surface ocean variables near reality. Hence, the ocean-atmosphere fluxes contain both,

the realistic fluxes and the response of the boundary layer model to incompatibilities of the "realistic" atmosphere data and the ocean model. So the momentum- and heat flux are also control quantities for the accuracy of the ocean model.

The REMO based simulations use ERA-40 as boundary values and an ocean climatology to calculate atmosphere-ocean boundary fluxes. This allows the atmosphere model to drift locally away from reality. Hence, the experiments based on these data should be considered as "climate" runs.

For the coupling the scheme provided by the *MOM-4*-code is used. From the atmosphere and the ocean surface state variables, momentum- and heat flux are calculated for a time segment in advance. The ocean variables are extrapolated in time (simply kept constant), the atmosphere variables are known and time interpolated values are used. The calculated fluxes are kept constant over the next time segment and are used to drive the ocean model. A coupling segment length of 1 hour is found as suitable.

6.2.2 Data flow

Spatial interpolation

The input data files are provided in netCDF format. During model initialisation the information on the input grid is analyzed to initialize the interpolation onto the ocean model grid. All surface fluxes are calculated after the interpolation with the resolution of the ocean grid. Each data file is interpolated separately, so mixed atmosphere data sets with different spatial resolution as QuikScat winds and NCEP data otherwise do not require additional data preprocessing.

Because the atmosphere grid is coarser than the ocean grid coastal ocean points may contain land data. This would imply unrealistic forcing near the coast. Especially the reanalyzed wind field may be too weak, since land surface roughness is larger than sea surface roughness.

Also scatterometer based data as QuikScat wind fields may be not valid at coastal points. Extrapolation of open ocean data to coastal point promise a quick solution. However, because coastal wind is generally modified by the influence of land, it is not clear whether or not such a procedure improves data. Currently, this problem has neglected and data at coastal points are used as they are.

There are a few missing data in the QuikScat data set. These gaps are filled by a nearest neighbor averaging procedure which is repeated until all gaps are closed. This method is monotonic and easy to implement. Because gaps are rare and also small in most cases more sophisticated methods are not appropriate.

Data are mapped to the ocean model grid in *MOM-4* using a bilinear interpolation method. This method is numerically fast and strictly monotonic. However, derivatives of interpolated fields may exhibit jumps at box boundaries of the coarse grid. This can be seen especially in the curl of the wind stress, which plays an important role in the open ocean via the Sverdrup balance, but is believed to rule also vertical velocity in the Benguela upwelling area. Hence, another method is used for the wind fields, which is based on bicubic interpolation, Press et al. (1992).

The bicubic method fails at the coast for Quikscat winds because land points are flagged as missing in this data set. Hence, a nearest neighbor averaging is used before interpolation to extrapolate the wind over the sea to land.

Figure 6.1 demonstrates the influence of the interpolation method on the imposed wind stress curl. The left hand figure shows the wind stress curl calculated directly on the coarse grid (NCEP) using central differences. The Figure in the middle shows the curl calculated on

the fine grid after bilinear interpolation from the coarse grid. A very unlikely feature are the artificial edges in the wind stress curl. The bicubic interpolation method gives much smoother results. However, it tends to enhance the wind stress curl calculated on the fine grid compared with the curl calculated directly on the coarse grid. In all experiments bicubic interpolation is used.

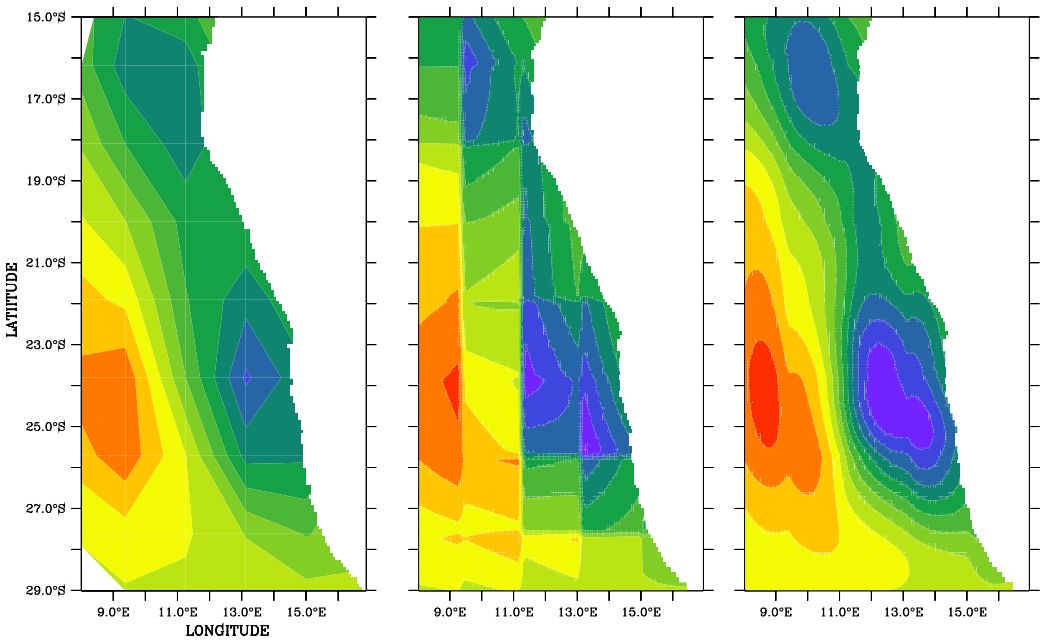

Fig. 6.1
The influence of interpolation on the wind stress curl.

Abb. 6.1
Der Einfluss der Interpolation der Windschubspannung.

Time interpolation

The atmosphere-ocean fluxes are calculated for every model hour. Data are interpolated linearly between two time steps in the input files in such a way, that the time integrals of the interpolated quantities are conserved. The *MOM-4* time interpolation module organizes the interpolation and determines, when a new time slice must be read. The interpolation is organized based on the time information in the input file. Hence, small gaps in the input files must not be filled with interpolated data.

6.2.3 Calculation of fluxes

The coupler of *MOM-4* uses bulk formula for the calculation of wind stress and heat fluxes, Beljaars (1994). However, short wave and long wave radiation must be prescribed, but are not delivered by all data sets. Below, methods to calculate surface fluxes are given in detail.

Wind stress

The vertical momentum flux $\vec{\tau}$ is related to the square of the wind speed $\vec{u}_w$,

$$\vec{\tau} = \rho_a \, C_D \, |u_{10}| \, \vec{u}_{10} \tag{6.1}$$

Currently, for the drag coefficient C_D the approximation

$$C_D = 10^{-3} \left(c_1 + c_2 \, |u_{10}| \right) \tag{6.2}$$

$$\rho_a = 1.22 \cdot 10^{-3} \mathrm{g\,cm^{-3}} \tag{6.3}$$

$$c_1 = 0.63 \tag{6.4}$$

$$c_2 = 0.066 \mathrm{s\,m^{-1}} \tag{6.5}$$

Smith & Banke (1975) is used. A more sophisticated approximation which accounts also for the stability of the atmosphere, Smith (1988), Kara et al. (2002), is also tested. Especially in the Benguela upwelling area, where warm air overlays cold upwelled water, reduced wind stress in a stratified atmosphere may by important. However, it is not clear how boundary layer stability is taken into account in the calculation of wind fields from scatterometer data. If this is based a neutral boundary layer, also a neutral bulk formula should be used for the wind stress calculation.

Insolation

The solar radiation is calculated in the boundary layer model,

$$Q_s = D \, C \, A \, T_0 \, S_0 \cos \eta \tag{6.6}$$

D accounts for the varying distance between sun and earth and is currently approximated as $D \approx 1$.

$$S_0 = 1370 \, \mathrm{W\,m^{-2}} \tag{6.7}$$

is the solar radiation at the top of the atmosphere. The sun angle η counted from zenith describes the astronomical variation of the insolation,

$$\cos \eta = \sin(\delta) \sin(\varphi) + \cos(\delta) \cos(\varphi) \cos(t). \tag{6.8}$$

φ is the latitude, δ is the declination of the sun and the t is the sun's hour angle, defined from the local time t_l by

$$t = \frac{\pi}{12 \, \mathrm{h}} t_l - \pi. \tag{6.9}$$

The local time t_l (in hours) depends on longitude λ and is derived from the model calendar,

$$t_l = 24 \, d_J + \frac{\lambda_r}{15} \tag{6.10}$$

$$\lambda_r = \begin{cases} \lambda & \text{for } \lambda < 180^\circ \\ \lambda - 360 & \text{for } \lambda > 180^\circ \end{cases} . \tag{6.11}$$

d_J is the Julian day. The declination δ is approximated by

$$\delta \approx 0.40927 \sin \left(\frac{2 \, \pi (d_J + 284 \, d)}{365.25 \, d} \right) . \tag{6.12}$$

The transmissivity T_0 is calculated following Bodin (1979). For the albedo A the Fresnel formula

$$A = \frac{1}{2}\left(\frac{\sin^2(\eta-\psi)}{\sin^2(\eta+\psi)} + \frac{\tan^2(\eta-\psi)}{\tan^2(\eta+\psi)}\right) \tag{6.13}$$

is used, the refraction angle ψ is approximated as

$$\psi = \arcsin\left(\frac{\sin(\eta)}{1.333}\right) \tag{6.14}$$

Thermal radiation budget

The long wave radiation budget has two constituents, the upwelling radiation S_u and the downwelling radiation S_d. The upwelling radiation consists of the radiation component emitted by the ocean, which is governed by Stefan-Boltzmann's law and by the reflected part of the downwelling radiation,

$$S_u = \delta\sigma T_s^4 + (1-\delta)\, S_d. \tag{6.15}$$

T_s is the sea surface temperature, $\sigma = 5.67032 \cdot 10^{-8}\,\mathrm{W\ m^{-2}K^{-4}}$ the Stefan-Boltzmann constant. $\delta \approx 0.95$ is the total emissivity of the ocean surface.
The downwelling radiation depends on the atmosphere temperature, water vapor content and cloud coverage of the sky,

$$S_d = \sigma T_a^4\,(1 - g(e_a, c)) \tag{6.16}$$

The total budget for the ocean is

$$Q_l = -(S_u - S_d) = -\delta\sigma\left(T_s^4 - T_a^4(1-g(e_a,c))\right). \tag{6.17}$$

Humidity and cloud correction are separated as usually by

$$g(e_a, c) = f(e_a)h(c). \tag{6.18}$$

Following Oberhuber (1988) the water vapor correction is given in terms of the water vapor pressure e_a,

$$f(e_a) = 0.39 - 0.05\sqrt{e_a/\mathrm{hPa}}. \tag{6.19}$$

For the cloud correction a several functions of the form

$$h(c) = (1 - dc), \tag{6.20}$$

$$h(c) = (1 - dc^2) \tag{6.21}$$

are currently tested. The quadratic formula results in a lower SST.

Sensible heat flux

The sensible heat flux is proportional to the temperature difference between ocean and atmosphere,

$$Q_s = C_T c_{p.air} |u_{10}| \rho_{a0}\,(T_a - T_s) \tag{6.22}$$

$c_{p.air} = 1005\,\mathrm{Ws\ kg^{-1}K^{-1}}$ is the specific heat of air, ρ_{a0} is the density of air. The coefficient $C_T = 1.1 \cdot 10^{-3}$ is kept constant, but will be varied in later experiments.

Latent heat flux

The latent heat flux is parameterized in terms of the water vapor pressure difference to the saturation water vapor pressure at sea surface temperature,

$$Q_L = C_E \, L \, |u_{10}| \frac{\rho_{a0}}{p_a} \frac{R_d}{R_w} \left(r \, e_a^{sat}(T_a) - e_a^{sat}(T_s) \right). \tag{6.23}$$

r is the relative humidity, e_a^{sat} the saturation water vapor pressure, p_a the air pressure, R_d and R_w are the gas constants of dry air and pure water vapor respectively, with

$$\frac{R_d}{R_w} \approx 0.622. \tag{6.24}$$

For the transition coefficient the approximation

$$C_E \approx 1.2 \, C_T \tag{6.25}$$

is used.

Heat entrainment with fresh water

Freshwater flux as rain usually has a different temperature than sea surface temperature. The corresponding heat flux is

$$Q_f = c_p \, \rho_w \, P \, T_r. \tag{6.26}$$

c_p is the specific heat of fresh water, ρ_w the density, P the precipitation rate in m s^{-1} and T_r the temperature of rain. The approximation $T_r \approx T_a$ is used.

A The time stepping scheme in *MOM-4*

A.1 Staggered time stepping

In *MOM-4* tracers and velocities are updated staggered in time (see Section 12.6 in Griffies, 2004)Griffies (2004). Velocity, $\mathbf{u}$, is given on integer time steps, τ, tracer fields, T, are defined on half integer time steps, $\tau + \Delta\tau/2$. Hence, the cell hight as well as the sea surface elevation are needed at both, integer and half integer time steps. *MOM-4* employs also a splitting between the baroclinic and barotropic mode. Together with the staggered time stepping this splitting needs special attention. Some details are unpublished and are given here.

A.2 Updating tracer and velocity variables

$$\frac{(hT)^{\tau+1/2} - (hT)^{\tau-1/2}}{\Delta\tau} = -\nabla_s \cdot \left[(h\mathbf{u})^{\tau} T^{\tau-1/2} + (h\mathbf{F})^{\tau-1/2}\right] \\ -\delta_k \left[w^{\tau} T^{\tau-1/2} + F_z^{\tau+1/2}\right] + h^{\tau-1/2} S_T^{\tau} - \delta_k w_{sink}^{\tau} T^{\tau+1/2} \tag{A.1}$$

h is the time dependent cell thickness for tracer T-cells (half integer time steps) and velocity $\mathbf{u}$-cells (integer time steps). The tracer advection velocity $(h\mathbf{u})^{\tau})$ and $w^{\tau}$is placed at horizontal and vertical cell interfaces. The time stepping is done with the positive "mdfl-sweby"-scheme,Hundsdorfer & Trompert (1994). Horizontal subgrid scale mixing is calculated explicitly, vertical subgrid scale mixing is updated implicitly. Vertical advection is also treated explicitly. However, for fast sinking of suspended matter but also for fast vertical migration of zooplankton with velocity w_{sink} an implicit scheme is required. The source term S_T^{τ} summarizes the complete ecosystem dynamics.

The horizontal baroclinic velocity $\mathbf{u}$ is updated like follows:

$$\frac{(h\mathbf{u})^{\tau+1} - (h\mathbf{u})^{\tau}}{\Delta\tau} = \left[-\nabla_s \cdot (h\mathbf{u}\mathbf{u}) - M\hat{z} \times (h\mathbf{u}) - \delta_k (w\mathbf{u})\right]_{AB} \\ -h^{\tau} \left[f\hat{z} \times \mathbf{u}\right]_{semi-implicit} - \frac{h^{\tau}}{\rho} \nabla_z p_s^{\tau+1/2} - \nabla_s \cdot (hF)^{\tau} - \delta_k F_z^{\tau+1} \tag{A.2}$$

advective terms are evaluated with an Admams-Bashford scheme, the Coriolis force semi-implicitly, horizontal subgrid scale viscosity explicitly and vertical subgrid scale viscosity by an implicit scheme.

The tracer and velocity update require $h^{\tau+1/2}$ and h^{τ} respectively. Hence, the vertically integrated quantities as well as the thickness of grid cells must be completed before the tracer and velocity fields can be updated.

A.3 Updating vertically integrated variables

The volume budget of a grid cell reads

$$\frac{\partial \eta}{\partial t} = -\nabla_s \cdot \mathbf{U} + q_w, \tag{A.3}$$

where η is the sea surface hight, q_w the fresh water volume flux and

$$\mathbf{U} = \int_{-H}^{\eta} dz \mathbf{u} \tag{A.4}$$

is the horizontally integrated vertical velocity that is updated like

$$\rho_0 \left(\frac{\partial}{\partial t} + f\hat{z}\times \right) \mathbf{U} = (H+\eta)\nabla_z p_s + \rho_0 G. \tag{A.5}$$

Here $p_s = \rho g \eta$ is the surface pressure and G the vertical integral of all remaining terms in Equation (A.2).

These barotropic equations are updated with a time step much smaller than the baroclinic time step. The information on the sea level and on the vertically integrated velocity is fed back to the baroclinic equations. Appropriate average methods help to reduce numerical noise. The surface hight and the barotropic velocity evaluated with the small time step are $\eta^b(\tau, t_n)$ and $\mathbf{U}^b(\tau, t_n)$. The time steps t_n are

$$t_n = \tau + n\Delta t, \tag{A.6}$$

hence, the barotropic time stepping proceeds from the initial time $t_0 = \tau$ to $t_N = \tau + 2\Delta\tau$, where the integer N is a function of the split between the barotropic and the baroclinic mode.

The basis of the barotropic time stepping is a predictor-corrector scheme. The first step "predicts" the surface height

$$\frac{\eta^\star(\tau, t_{n+1}) - \eta^b(\tau, t_n)}{\gamma \Delta t} = -\nabla_s \cdot \mathbf{U^b}(\tau, \mathbf{t_n}) + q_w(\tau + \Delta\tau/2), \tag{A.7}$$

The raised $(\star)$ denotes the intermediate value. The value of the parameter γ may vary, but has kept to its default value of $\gamma = 0.2$ here. More details on the implemented predictor-corrector scheme can be found in Section 12.8 of Griffies, 2004, GRIFFIES (2004). From the "predicted" surface height the surface pressure is computed,

$$\rho_0 p_s^\star(\tau, t_{n+1}) = g\eta^\star(\tau, t_{n+1})\rho_{k=1}(\tau + 1/2), \tag{A.8}$$

that in turn is used to update the vertically integrated velocity,

$$\begin{aligned} \frac{\mathbf{U}^b(\tau, t_{n+1}) - \mathbf{U}^b(\tau, t_n)}{\Delta t} = &-f\hat{z}\frac{\mathbf{U}^b(\tau, t_{n+1}) + \mathbf{U}^b(\tau, t_n)}{2} \\ &-(H + \eta(\tau))\nabla_z p_s^\star(\tau, t_{n+1}) + G(\tau). \end{aligned} \tag{A.9}$$

The following "corrector" step finalises the surface height from the updated transport,

$$\eta^b(\tau, t_{n+1}) - \eta^b(\tau, t_n) = \Delta t F(t_{n+1}), \tag{A.10}$$

with

$$F(t_n) = \nabla_s \cdot \mathbf{U}^b(\tau, t_n) + q_w(\tau + \Delta\tau/2). \tag{A.11}$$

Now we describe the scheme, how appropriate averages of η^b and $\mathbf{U}^b$ are coupled back to the baroclinic and tracer scheme. The repeated application of the barotropic scheme gives

$$\eta^b(\tau, t_n) = \eta(\tau) + \Delta t \sum_{i=1}^{n} F(t_i), \tag{A.12}$$

and the accumulation of N barotropic time step leads to

$$\frac{\eta^b(\tau, t_N) - \eta^b(\tau, t_0)}{N\Delta t} = \frac{1}{N} \sum_{n=1}^{N} F(t_n). \tag{A.13}$$

A time average over the full suite of barotropic surface heights provides a smooth approximation for the sea surface height,

$$\eta(\tau + \Delta\tau) = \frac{1}{N+1} \sum_{n=0}^{N} \eta^b(\tau, t_n. \tag{A.14}$$

Combining these expressions and keeping in mind that a barotropic sequence starts with $\eta^b(\tau, t_0) = \eta(\tau)$ and using $N\Delta t = 2\Delta\tau$ the sea surface height for the baroclinic mode reads

$$\eta(\tau + \Delta\tau) - \eta(\tau) = \frac{2\Delta\tau}{N(N+1)} \sum_{n=1}^{N} \sum_{n=1}^{n} F(t_i). \tag{A.15}$$

The double sum can be replaced by a single sum that is more appropriate to accumulate the barotropic results during the barotropic steps,

$$\sum_{n=1}^{N} \sum_{n=1}^{n} F(t_i) = \sum_{n=1}^{N} (N - n + 1) F(t_n). \tag{A.16}$$

This gives

$$\eta(\tau + \Delta\tau) - \eta(\tau) = \Delta\tau \bar{F}(\tau), \tag{A.17}$$

$$\bar{F}(\tau) = \frac{2}{N(N+1)} \sum_{n=1}^{N} (N - n + 1) F(t_n). \tag{A.18}$$

Finally $\mathbf{U}$ needs to be defined. It is approximated as

$$\mathbf{U}(\tau + \Delta\tau) = \frac{2\Delta\tau}{N(N+1)} \sum_{n=1}^{N} (N - n + 1) \mathbf{U}^b(\tau, t_n). \tag{A.19}$$

The half integer surface height required for the consistent update of the tracer equations reads

$$\eta(\tau + \Delta\tau/2) = \eta(\tau - \Delta\tau/2) + \Delta\tau \left(-\nabla_s \cdot \mathbf{U}(\tau) + q_w(\tau) \right). \tag{A.20}$$

Acknowledgment

The authors acknowledge use of the Ferret program for analysis and graphics in this paper. Ferret is a product of NOAA's Pacific Marine Environmental Laboratory. (Information is available at www.ferret.noaa.gov)

QuikScat data are produced by Remote Sensing Systems and sponsored by the NASA Ocean Vector Winds Science Team. Data are available at www.remss.com.

NCEP reanalysis data are provided by the NOAA-CIRES Climate Diagnostics Center, Boulder, Colorado, USA, from their Web site at http://www.cdc.noaa.gov/.

The "Ecco" data are a contribution of the Consortium for Estimating the Circulation and Climate of the Ocean (ECCO) funded by the National Oceanographic Partnership Program.

Stefan Schäfer has investigated the analytical properties of the Anammox process and developed the functions and has adjusted the slope parameters (see section 3.4.4).

This project is partly supported by the BMBF, grant 03G0580A.

Bibliography

Arrigo, K.R.: 2005: Marine microorganisms and global nutrient cycles Nature **437**, 349–355.

Beljaars, A.C.M.: 1994: The parameterization of surface fluxes in large-scale models under free convection Q. j. roy. meteor. soc. **121**, 255–270.

Blanchard, F., Guarini, J.M., Richard, P., Gros, P., Mornet, F.: 1996: Quantifying the short-term temperature effect on light-saturated photosynthesis of intertidal microphytobenthos Mar. ecol. prog. ser. **134**, 309–313.

Bodin, S.: 1979: A predictive numerical model of the atmospheric boundary layer based on the turbulent energy equation Technical Report SE-60176 Swedish Meteorological and Hydrological Institute.

Boyd, A.J., Salat, J., Maso, M.: 1987: The seasonal intrusion of relatively saline water on the shelf of northern and central namibia S. afr. j. marine sci. , 107–120.

Brüchert, V., Jorgensen, B.B., Neumann, K., Riechmann, D., Schlösser, M., Schulz, H.: 2003: Regulation of bacterial sulfate reduction and hydrogen sulfide fluxes in the central namibian coastal upwelling zone and Geochim. cosmochim. ac. **67**, 4505–4518.

Bryan, K., Lewis, L.J.: 1979: A water mass model of the world ocean and J. geophys. res. **84**, 2503–2517.

Chapman, P., Shannon, L.V.: 1985: The benguela ecosystem part ii. chemistry and related processes Oceanogr. mar. biol. **23**, 183–251.

Conkright, M.E., Locarnini, R.A., Garcia, H.E., O'Brien, T.D., Boyer, T.P., Stephens, C., Antonov, J.I.: 2002: World ocean atlas 2001: Objective analyses and data statistics and and figures and cd-rom documentation Technical report National Oceanographic Data Center Silver Spring and MD.

Dalsgaard, T., Canfield, D.E., Petersen, J., Thamdrup, B., Acuna-Gonzalez, J.: 2003: n_2 production by the anammox reaction in the anoxic water column of golfo dulce and costa rrica Nature **422**, 606–608.

Deutsch, C., Sarmiento, J.L., Sigman, D.M., Gruber, N., Dunne, J.P.: 2007: Spatial coupling of nitrogen inputs and losses in the ocean Nature **445**, 163–167.

Devol, A.H.: 2003: Nitrogen cycle: Solution to a marine mystery Nature **422**, 575–576.

Dunker, R.: 2005: Microsensor studies on a *Beggiatoa* mat under changing oxygen concentrations Master's thesis University of Bremen.

Emery, W.J., Lee, W.G., Maagard, L.: 1984: Geographical and seasonal distribution of brunt-väisälä frequency and rossby radii in the north pacific and north atlantic J. phys. oceanogr. **14**, 294–317.

Fennel, W., Neumann, T.: 1996: The mesoscale variability of nutrients and plankton as seen in a coupled model Ger. j. hydrogr. **48**, 49–71.

Fennel, W., Neumann, T.: 2004: Introduction to the Modelling of Marine Ecosystems Elsevier and Amsterdam.

Geider, R.J., MacIntyre, H.L., Kana, T.M.: 1997: A dynamic of phytoplankton growth and acclimation: Responses of the balanced growth rate of chlorophyll a : carbon ratio to light, nutrientlimitation, and temperature Mar. ecol. prog. ser. **148**, 187–200.

Gentleman, W.C., Neuheimer, A.B.: 2008: Functional responses and ecosystem dynamics: How clearance rates explain the influence of satiation and food-limitation and acclimation J. plankton res. **30**, 1215–1231.

Griffies, S.M.: 2009: Elements of *mom4p1*, GFDL Ocean Group Technical Report Technical Report 6 NOAA/Geophysical Fluid Dynamics Laboratory.

Griffies, S.M., Pacanowski, R.C., Schmidt, M., Balaji, V.: 2001: Tracer conservation with an explicit free surface method for z-coordinate ocean models Mon. weather rev. **129**, 1081–1098.

Griffies, S.M.: 2004: Fundamentals of ocean climate models Princeton, USA: Princeton University Press 500 pp + index.

Gunnars, A., Blomqvist, S.: 1997: Phosphate exchange across the sediment-water interface when shifting from anoxic to oxic conditions an experimental comparison of freshwater and brackish-marine systems Biogeochemistry **37**, 203–226.

Herzfeld, M., Schmidt, M., Griffies, S., Liang, Z.: 2011: Realistic test cases for limited area ocean modelling Ocean model. **37**, 1–34.

Hundsdorfer, W., Trompert, R.A.: 1994: Method of lines and direct discretization: a comparison for linear advection Appl. numer. math. **13**, 469–490.

Jackett, D.R., McDougall, T.J., Feistel, R., Wright, D.G., Griffies, S.M.: 2006: Algorithms for density, potential temperature, conservative temperature, and freezing temperature of seawater J. atmos. ocean tech. **23**, 1709 –1728.

Kara, A.B., Rochford, P.A., Hurlburt, H.E.: 2002: Air-sea flux estimates and the 1997-1998 enso event Bound.-lay. meteorol. **103**, 439–458.

Kriest, I., Oschlies, A.: 2007: On the treatment of particulate organic matter sinking in large-scale models of marine biogeochemical cycles Biogeosciences d. **4**, 3005–3040.

Kuypers, M.M., Lavik, G., Woebken, D., Schmid, M., Fuchs, B., Amann, R., Joergensen, B.B., Jetten, M.S.M.: 2005: Massive nitrogen loss from the benguela upwelling system through anaerobic ammonium oxidation P. natl. acad. sci. **102**, 6478–6483.

Lam, P., Lavik, G., Jensen, M.M., van de Vossenberg, J., Schmid, M., Woebken, D., Gutierrez, D., Amann, R., Jetten, M.S.M., Kuypers, M.M.: 2009: Revising the nitrogen cycle in the peruvian oxygen minimum zone P. natl. acad. sci. **106**, 4752–4757.

Large, W.G., McWilliams, J.C., Doney, S.C.: 1994: Oceanic vertical mixing: A review and a model with a nonlocal boundary layer parameterization Rev. geophys. **32**, 363–403.

LaRoche, J., Breitbarth, E.: 2005: Importance of the diazotrophs as a source of new nitrogen in the ocean J. Sea. res. **53**, 67–91.

Lass, H.U., Mohrholz, V.: 2005: On the fluctuations and vertical structure of the shelf circulation off walvis bay and namibia Cont. shelf res. **25**, 1473–1497.

Lass, H.U., Mohrholz, V.: 2008: On the interaction between the subtropical gyre and the subtropical cell on the shelf of the se atlantic J. mar. sys. **74**, 1–43.

Lavik, G., Stührmann, T., Brüchert, V., van der Plas, A., Mohrholz, V., Lam, P., Mussmann, M., Fuchs, B.M., Amann, R., Lass, U., Kuypers, M.M.M.: 2009: Detoxification of sulphidic african shelf waters by blooming chemolithotrophs Nature **457**, 581–585.

Li, Q.P., Franks, P.J.S., Landry, M.R., Goericke, R., Taylor, A.G.: 2010: Modeling phytoplankton growth rates and chlorophyll to carbon ratios in california coastal and pelagic ecosystems J. geophys. res. **115**, 1–12.

Mohrholz, V., Bartholomae, C.H., van der Plas, A.K., Lass, H.U.: 2008: The seasonal variability of the northern benguela undercurrent and its relation to the oxygen budget on the shelf Cont. shelf res. **28**, 424–441.

Moller, E.F.: 2005: Sloppy feeding in marine copepods: prey-size-dependent production of dissolved organic carbon J. plankton res. **27**, 27–35.

Monteiro, P.M., van der Plas, A.K., Mohrholz, V., Mabille, E., Pascall, A., Joubert, W.: 2006: Variability of natural hypoxia and methane in a coastal upwelling system: Oceanic physics or shelf biology? Geophys. res. lett. **33**, 111–222.

Neumann, T., Schernewski, G.: 2008: Eutrophication in the baltic sea and shifts in nitrogen fixation analyzed with a 3d ecosystem model J. mar. sys. **74**, 592–602.

Nicholls, J.C., Davies, C.A., Trimmer, M.: 2007: High-resolution profiles and nitrogen isotope tracing reveal a dominant source of nitrous oxide and multiple pathways of nitrogen gas formation in the central arabian sea Limnol. oceanogr. **52**, 156–168.

NOAA, N.G.D.C.: 1988: Data announcement 88-mgg-02, digital relief of the surface of the earth Technical report Technical report of NOAA, National Geophysical Data Center, Boulder, Colorado.

Oberhuber, J.M.: 1988: An atlas based on the "coads" data set: The budgets of heat and buoyancy and turbulent kinetic energy at the surface of the global ocean Technical Report 15 Max-Plack-Institut für Meteorologie.

Pacanowski, R.C., Griffies, S.M.: 2000: Mom 3.0 manual Technical report Geophysical Fluid Dynamics Laboratory and Princeton and USA.

Pacanowski, R.C., Philander, S.G.H.: 1981: Parameterization of vertical mixing in numerical models of tropical oceans J. phys. oceanogr. **11**, 1443–1451.

Peters, H., Gregg, M.C., Toole, J.M.: 1988: On the parameterization of equatorial tubulence J. geophys. res. **93**, 1199–1218.

Pitcher, G.C., Boyd, A.J., Horstman, D.A., Mitchell-Innes, B.A.: 1998: Subsurface dinoflagellate populations and frontal blooms and the formation of red tide in the southern benguela upwelling system Mar. ecol. prog. ser. **172**, 253–264.

Platt, T.C., Gallegos, L., Harrison, W.G.: 1980: Photoinhibition of photosynthesis in natural assemblages of marine phytoplankton J. mar. res. **38**, 687–701.

Preisler, A., de Beer, D., Lichtschlag, A., Lavik, G., Boetius, A., Jorgensen, B.B.: 2007: Biological and chemical sulfide oxidation in a beggiatoa inhabited marine sediment ISME j. **1**, 341–353.

Press, W.H., Teukolsky, S.A., Vetterling, W.T., Flannery, B.P.: 1992: Numerical Recipes in FORTRAN: The Art of Scientific Computing Cambridge University Press and Cambridge.

Rees, A.P., Woodward, E.M.S., Joint, I.: 2006: Concentrations and uptake of nitrate and ammonium in the atlantic ocean between 60°n and 50°s Deep-Sea res. pt. II **53**, 1649–1665.

Richards, F.A.: 1965: Chemical Oceanography chapter Anoxic basins and fjords Academic Press and London 611–643.

Schäfer, H.T., Ferdelman, G., Fossing, H., Muyzer, G.: 2008: Microbial diversity in deep sediments of the benguela upwelling system Aquat. microb. ecol. **50**, 1–9.

Schulz, H., Brinkhoff, H., Ferdelman, T.G., Hernandez, M.M., Teske, A., Jorgensen, B.B.: 1999: Dense population of a giant sulfur bacterium in namibian shelf sediments Science **284**, 493–495.

Smagorinsky, J.: 1963: General circulation experiments with the primitive equations: I. the basic experiment Mon. weather rev. **91**, 99–164.

Smith, S.D.: 1988: Coefficients for sea surface wind stress and heat flux and and wind profiles as a function of wind speed and temperature J. geophys. res. **93**, 467–472.

Smith, S.D., Banke, E.G.: 1975: Variation of the sea surface drag coefficient with wind speed Q. j. roy. meteor. soc. **101**, 665–673.

Sohm, J.A., Hilton, J.A., Noble, A.E., Zehr, J.P., Saito, M.A., Webb, E.A.: 2011: Nitrogen fixation in the south atlantic gyre and the benguela upwelling system Geophys. res. lett. **38**, L16608.

Stacey, M.W., Pond, S., Nowak, Z.P.: 1995: A numerical model of the circulation in knight inlet, british columbia, canada J. phys. oceanogr. **25**, 1037–1062.

Steele, J.: 1962: Environmental control of photosynthesis in the sea Limnol. oceanogr. **7**, 137–150.

Stigebrandt, A., Wulff, F.: 1987: A model for the dynamics of nutrients and oxygen in the baltic proper J. mar. res. **45**, 729–759.

Tyrrell, T., Lucas, M.I.: 2002: Geochemical evidence of denitrification in the benguela upwelling system Cont. shelf res. **22**, 2497–2511.

Voss, M., Montoya, J.P.: 2009: Nitrogen cycle: Oceans apart Nature **461**, 49–50.

Walsby, A.E.: 1997: Numerical integration of phytoplankton photosynthesis through time and depth in a water column New phytol. **136**, 189–209.

Walsh, D.A., Zaikova1, E., Howes, C.G., Song, Y.C., Wright, J.J., Tringe, S.G., Tortell, P.D., Hallam, S.J.: 2009: Metagenome of a versatile chemolithoautotroph from expanding oceanic dead zones Science **326**, 578–582.

Wasmund, N., Lass, H.U., Nausch, G.: 2005: Distribution of nutrients, chlorophyll and phytoplankton primary production in relation to hydrographic structures bordering the benguela-angolan frontal region Afr. j. mar. sci. **27**, 177–190.

Watermeyer, K.E., Shannon, L.J., Griffiths, C.L.: 2008a: Changes in the trophic structure of the southern benguela before and after the onset of industrial fishing Afr. j. mar. sci. **30**, 351–382.

Watermeyer, K.E., Shannon, L.J., Roux, J.P., Griffiths, C.L.: 2008b: Changes in the trophic structure of the southern benguela before and after the onset of industrial fishing Afr. j. mar. sci. **30**, 383–403.

Webb, W.L., Newton, M., Starr, D.: 1974: Carbon dioxide exchange of *Calnus rubra*: Mathematical model Oecologia **17**, 281–291.

Wessel, P., Smith, W.H.F.: 1996: A global self-consistent and hierarchical and high-resolution shoreline database J. geophys. res. **101**, 8741–8743.

Wright, J.J., Konwar, K.M., Hallam, S.J.: 2012: Microbial ecology of expanding oxygen minimum zones Nat. rev. microbiol. **10**, 381–394.

Yool, A., Martin, A.P., Fernandez, C., Clark, D.R.: 2007: The significance of nitrification for oceanic new production Nature **447**, 999–1002.

Meereswissenschaftliche Berichte

MARINE SCIENCE REPORTS

1 (1990) Postel, Lutz:
Die Reaktion des Mesozooplanktons, speziell der Biomasse, auf küstennahen Auftrieb vor Westafrika (The mesozooplankton response to coastal upwelling off West Africa with particular regard to biomass)

2 (1990) Nehring, Dietwart:
Die hydrographisch–chemischen Bedingungen in der westlichen und zentralen Ostsee von 1979 bis 1988 – ein Vergleich (Hydrographic and chemical conditions in the western and central Baltic Sea from 1979 to 1988 – a comparison)
Nehring, Dietwart; Matthäus, Wolfgang:
Aktuelle Trends hydrographischer und chemischer Parameter in der Ostsee, 1958 – 1989 (Topical trends of hydrographic and chemical parameters in the Baltic Sea, 1958 – 1989)

3 (1990) Zahn, Wolfgang:
Zur numerischen Vorticityanalyse mesoskaler Strom- und Massenfelder im Ozean (On numerical vorticity analysis of mesoscale current and mass fields in the ocean)

4 (1992) Lemke, Wolfram; Lange, Dieter; Endler, Rudolf (Eds.):
Proceedings of the Second Marine Geological Conference – The Baltic, held in Rostock from October 21 to October 26, 1991

5 (1993) Endler, Rudolf; Lackschewitz, Klas (Eds.):
Cruise Report RV "Sonne" Cruise SO82, 1992

6 (1993) Kulik, Dmitri A.; Harff, Jan:
Physicochemical modeling of the Baltic Sea water–sediment column: I. Reference ion association models of normative seawater and of Baltic brackish waters at salinities 1–40 ‰, 1 bar total pressure and o to 30 C temperature
(system Na–Mg–Ca–K–Sr–Li–Rb–Cl–S–C–Br–F–B–N–Si– P–H–O)

7 (1994) Nehring, Dietwart; Matthäus, Wolfgang; Lass, Hans Ulrich; Nausch, Günther:
Hydrographisch–chemische Zustandseinschätzung der Ostsee 1993

8 (1995) Hagen, Eberhard; John, Hans-Christian:
Hydrographische Schnitte im Ostrandstromsystem vor Portugal und Marokko 1991 - 1992

9 (1995) Nehring, Dietwart; Matthäus,Wolfgang; Lass, Hans Ulrich; Nausch, Günther; Nagel, Klaus:
Hydrographisch-chemische Zustandseinschätzung der Ostsee 1994
Seifert, Torsten; Kayser, Bernd:
A high resolution spherical grid topography of the Baltic Sea

10 (1995) Schmidt, Martin:
Analytical theory and numerical experiments to the forcing of flow at isolated topographic features

11 (1995) Kaiser, Wolfgang; Nehring, Dietwart; Breuel, Günter; Wasmund, Norbert; Siegel, Herbert; Witt, Gesine; Kerstan, Eberhard; Sadkowiak, Birgit:
Zeitreihen hydrographischer, chemischer und biologischer Variablen an der Küstenstation Warnemünde (westliche Ostsee)
Schneider, Bernd; Pohl, Christa:
Spurenmetallkonzentrationen vor der Küste Mecklenburg-Vorpommerns

12 (1996) Schinke, Holger:
Zu den Ursachen von Salzwassereinbrüchen in die Ostsee

13 (1996) Meyer-Harms, Bettina:
Ernährungsstrategie calanoider Copepoden in zwei unterschiedlich trophierten Seegebieten der Ostsee (Pommernbucht, Gotlandsee)

14 (1996) Reckermann, Marcus:
Ultraphytoplankton and protozoan communities and their interactions in different marine pelagic ecosystems (Arabian Sea and Baltic Sea)

15 (1996) Kerstan, Eberhard:
Untersuchung der Verteilungsmuster von Kohlenhydraten in der Ostsee unter Berücksichtigung produktionsbiologischer Meßgrößen

16 (1996) Nehring, Dietwart; Matthäus, Wolfgang; Lass, Hans Ulrich; Nausch, Günther; Nagel, Klaus:
Hydrographisch-chemische Zustandseinschätzung der Ostsee 1995

17 (1996) Brosin, Hans-Jürgen:
Zur Geschichte der Meeresforschung in der DDR

18 (1996) Kube, Jan:
The ecology of macrozoobenthos and sea ducks in the Pomeranian Bay

19 (1996) Hagen, Eberhard (Editor):
GOBEX - Summary Report

20 (1996) Harms, Andreas:
Die bodennahe Trübezone der Mecklenburger Bucht unter besonderer Betrachtung der Stoffdynamik bei Schwermetallen

21 (1997) Zülicke, Christoph; Hagen, Eberhard:
GOBEX Report - Hydrographic Data at IOW

22 (1997) Lindow, Helma:
Experimentelle Simulationen windangeregter dynamischer Muster in hochauflösenden numerischen Modellen

23 (1997) Thomas, Helmuth:
Anorganischer Kohlenstoff im Oberflächenwasser der Ostsee

24 (1997) Matthäus, Wolfgang; Nehring, Dietwart; Lass, Hans Ulrich; Nausch, Günther; Nagel, Klaus; Siegel, Herbert:
Hydrographisch-chemische Zustandseinschätzung der Ostsee 1996

25 (1997) v. Bodungen, Bodo; Hentzsch, Barbara (Herausgeber):
Neue Forschungslandschaften und Perspektiven der Meeresforschung - Reden und Vorträge zum Festakt und Symposium am 3. März 1997.

26 (1997) Lakaschus, Sönke:
Konzentrationen und Depositionen atmosphärischer Spurenmetalle an der Küstenstation Arkona

27 (1997) Löffler, Annekatrin:
Die Bedeutung von Partikeln für die Spurenmetallverteilung in der Ostsee, insbesondere unter dem Einfluß sich ändernder Redoxbedingungen in den zentralen Tiefenbecken

28 (1998) Leipe, Thomas; Eidam, Jürgen; Lampe, Reinhard; Meyer, Hinrich; Neumann, Thomas; Osadczuk, Andrzej; Janke, Wolfgang; Puff, Thomas; Blanz, Thomas; Gingele, Franz Xaver; Dannenberger, Dirk; Witt, Gesine:
Das Oderhaff. Beiträge zur Rekonstruktion der holozänen geologischen Entwicklung und anthropogenen Beeinflussung des Oder-Ästuars.

29 (1998) Matthäus, Wolfgang; Nausch, Günther; Lass, Hans Ulrich; Nagel, Klaus; Siegel, Herbert:
Hydrographisch-chemische Zustandseinschätzung der Ostsee 1997

30 (1998) Fennel, Katja:
Ein gekoppeltes, dreidimensionales Modell der Nährstoff- und Planktondynamik für die westliche Ostsee

31 (1998) Lemke, Wolfram:
Sedimentation und paläogeographische Entwicklung im westlichen Ostseeraum (Mecklenburger Bucht bis Arkonabecken) vom Ende der Weichselvereisung bis zur Litorinatransgression

32 (1998) Wasmund, Norbert; Alheit, Jürgen; Pollehne, Falk; Siegel, Herbert; Zettler, Michael L.:
Ergebnisse des Biologischen Monitorings der Ostsee im Jahre 1997 im Vergleich mit bisherigen Untersuchungen

33 (1998) Mohrholz, Volker:
Transport- und Vermischungsprozesse in der Pommerschen Bucht

34 (1998) Emeis, Kay-Christian; Struck, Ulrich (Editors):
Gotland Basin Experiment (GOBEX) - Status Report on Investigations concerning Benthic Processes, Sediment Formation and Accumulation

35 (1999) Matthäus, Wolfgang; Nausch, Günther; Lass, Hans Ulrich; Nagel, Klaus; Siegel, Herbert:
Hydrographisch-chemische Zustandseinschätzung der Ostsee 1998

36 (1999) Schernewski, Gerald:
Der Stoffhaushalt von Seen: Bedeutung zeitlicher Variabilität und räumlicher Heterogenität von Prozessen sowie des Betrachtungsmaßstabs - eine Analyse am Beispiel eines eutrophen, geschichteten Sees im Einzugsgebiet der Ostsee (Belauer See, Schleswig-Holstein)

37 (1999) Wasmund, Norbert; Alheit, Jürgen; Pollehne, Falk; Siegel, Herbert, Zettler, Michael L.:
Der biologische Zustand der Ostsee im Jahre 1998 auf der Basis von Phytoplankton-, Zooplankton- und Zoobenthosuntersuchungen

38 (2000) Wasmund, Norbert; Nausch, Günther; Postel, Lutz; Witek, Zbigniew; Zalewski, Mariusz; Gromisz, Sławomira; Łysiak-Pastuszak, Elżbieta; Olenina, Irina; Kavolyte, Rima; Jasinskaite, Aldona; Müller-Karulis, Bärbel; Ikauniece, Anda; Andrushaitis, Andris; Ojaveer, Henn; Kallaste, Kalle; Jaanus, Andres:
Trophic status of coastal and open areas of the south-eastern Baltic Sea based on nutrient and phytoplankton data from 1993 - 1997

39 (2000) Matthäus, Wolfgang; Nausch, Günther; Lass, Hans Ulrich; Nagel, Klaus; Siegel, Herbert:
Hydrographisch-chemische Zustandseinschätzung der Ostsee 1999

40 (2000) Schmidt, Martin; Mohrholz, Volker; Schmidt, Thomas; John, H.-Christian; Weinreben, Stefan; Diesterheft, Henry; Iita, Aina; Filipe, Vianda; Sangolay, Bomba-Bazik; Kreiner, Anja; Hashoongo, Victor; da Silva Neto, Domingos:
Data report of R/V "Poseidon" cruise 250 ANDEX'1999

41 (2000) v. Bodungen, Bodo; Dannowski, Ralf; Erbguth, Wilfried; Humborg, Christoph; Mahlburg, Stefan; Müller, Chris; Quast, Joachim; Rudolph, K.-U.; Schernewski, Gerald; Steidl, Jörg; Wallbaum, Volker:
Oder Basin - Baltic Sea Interactions (OBBSI): Endbericht

42 (2000) Zettler, Michael L.; Bönsch, Regine; Gosselck, Fritz:
Verbreitung des Makrozoobenthos in der Mecklenburger Bucht (südliche Ostsee) - rezent und im historischen Vergleich

43 (2000) Wasmund, Norbert; Alheit, Jürgen; Pollehne, Falk; Siegel, Herbert:
Der biologische Zustand der Ostsee im Jahre 1999 auf der Basis von Phytoplankton- und Zooplanktonuntersuchungen

44 (2001) Eichner, Christiane:
Mikrobielle Modifikation der Isotopensignatur des Stickstoffs in marinem partikulären Material

45 (2001) Matthäus, Wolfgang; Nausch, Günther (Editors):
The hydrographic-hydrochemical state of the western and central Baltic Sea in 1999/2000 and during the 1990s

46 (2001) Wasmund, Norbert; Pollehne, Falk; Postel, Lutz; Siegel, Herbert; Zettler, Michael L.:
Biologische Zustandseinschätzung der Ostsee im Jahre 2000

47 (2001) Lass, Hans Ulrich; Mohrholz, Volker; Nausch, Günther; Pohl, Christa; Postel, Lutz; Rüß, Dietmar; Schmidt, Martin; da Silva, Antonio; Wasmund, Norbert:
Data report of R/V "Meteor" cruise 48/3 ANBEN'2000

48 (2001) Schöner, Anne Charlotte:
Alkenone in Ostseesedimenten, -schwebstoffen und -algen: Indikatoren für das Paläomilieu?

49 (2002) Nausch, Günther; Feistel, Rainer; Lass, Hans Ulrich; Nagel, Klaus; Siegel, Herbert:
Hydrographisch-chemische Zustandseinschätzung der Ostsee 2001
Pohl, Christa; Hennings, Ursula:
Ostsee-Monitoring - Die Schwermetall-Situation in der Ostsee im Jahre 2001

50 (2002) Manasreh, Riyad:
The general circulation and water masses characteristics in the Gulf of Aqaba and northern Red Sea

51 (2002) Wasmund, Norbert; Pollehne, Falk; Postel, Lutz; Siegel, Herbert; Zettler, Michael L.:
Biologische Zustandseinschätzung der Ostsee im Jahre 2001

52 (2002) Reißmann, Jan Hinrich:
Integrale Eigenschaften von mesoskaligen Wirbelstrukturen in den tiefen Becken der Ostsee

53 (2002) Badewien, Thomas H.:
Horizontaler und vertikaler Sauerstoffaustausch in der Ostsee

54 (2003) Fennel, Wolfgang; Hentzsch, Barbara (Herausgeber):
Festschrift zum 65. Geburtstag von Wolfgang Matthäus

55 (2003) Nausch, Günther; Feistel, Rainer; Lass, Hans Ulrich; Nagel, Klaus; Siegel, Herbert:
Hydrographisch-chemische Zustandseinschätzung der Ostsee 2002
Pohl, Christa; Hennings, Ursula:
Die Schwermetall-Situation in der Ostsee im Jahre 2002

56 (2003) Wasmund, Norbert; Pollehne, Falk; Postel, Lutz; Siegel, Herbert; Zettler, Michael L.:
Biologische Zustandseinschätzung der Ostsee im Jahre 2002

57 (2004) Schernewski, Gerald; Dolch, Tobias (Editors):
The Oder estuary against the background of the European Water Framework Directive

58 (2004) Feistel, Rainer; Nausch, Günther; Matthäus, Wolfgang; Łysiak-Pastuszak, Elżbieta; Seifert, Torsten; Sehested Hansen, Ian; Mohrholz, Volker; Krüger, Siegfried; Buch, Erik; Hagen, Eberhard:
Background Data to the Exceptionally Warm Inflow into the Baltic Sea in late Summer of 2002

59 (2004) Nausch, Günther; Feistel, Rainer; Lass, Hans Ulrich; Nagel, Klaus; Siegel, Herbert:
Hydrographisch-chemische Zustandseinschätzung der Ostsee 2003
Pohl, Christa; Hennings, Ursula:
Die Schwermetall-Situation in der Ostsee im Jahre 2003

60 (2004) Wasmund, Norbert; Pollehne, Falk; Postel, Lutz; Siegel, Herbert; Zettler, Michael L.:
Biologische Zustandseinschätzung der Ostsee im Jahre 2003

61 (2004) Petry, Carolin:
Mikrobieller Abbau von partikulärem organischen Material in der tiefen Wassersäule

62 (2005) Nausch, Günther; Feistel, Rainer; Lass, Hans Ulrich; Nagel, Klaus; Siegel, Herbert:
Hydrographisch-chemische Zustandseinschätzung der Ostsee 2004
Pohl, Christa; Hennings, Ursula:
Die Schwermetall-Situation in der Ostsee im Jahre 2004

63 (2005) Umlauf, Lars; Burchard, Hans; Bolding, Karsten:
GOTM – Scientific Documentation. Version 3.2

64 (2005) Wasmund, Norbert; Pollehne, Falk; Postel, Lutz; Siegel, Herbert; Zettler, Michael L.:
Biologische Zustandseinschätzung der Ostsee im Jahre 2004

65 (2006) Matthäus, Wolfgang:
The history of investigation of salt water inflows into the Baltic Sea - from the early beginning to recent results

66 (2006) Nausch, Günther; Feistel, Rainer; Lass, Hans Ulrich; Nagel, Klaus; Siegel, Herbert:
Hydrographisch-chemische Zustandseinschätzung der Ostsee 2005
Pohl, Christa; Hennings, Ursula:
Die Schwermetall-Situation in der Ostsee im Jahre 2005

67 (2006) Rößler, Doreen:
Reconstruction of the Littorina Transgression in the Western Baltic Sea

68 (2006) Yakushev, Evgeniy V.; Pollehne, Falk; Jost, Günter; Kuznetsov, Ivan; Schneider, Bernd; Umlauf, Lars:
Redox Layer Model (ROLM): a tool for analysis of the water column oxic/anoxic interface processes

69 (2006) Wasmund, Norbert; Pollehne, Falk; Postel, Lutz; Siegel, Herbert; Zettler, Michael L.:
Biologische Zustandseinschätzung der Ostsee im Jahre 2005

70 (2007) Nausch, Günther; Feistel, Rainer; Lass, Hans Ulrich; Nagel, Klaus; Siegel, Herbert:
Hydrographisch-chemische Zustandseinschätzung der Ostsee 2006
Pohl, Christa; Hennings, Ursula:
Die Schwermetall-Situation in der Ostsee im Jahre 2006

71 (2007) Wasmund, Norbert; Pollehne, Falk; Postel, Lutz; Siegel, Herbert; Zettler, Michael L.:
Biologische Zustandseinschätzung der Ostsee im Jahre 2006

72 (2008) Nausch, Günther; Feistel, Rainer; Umlauf, Lars; Nagel, Klaus; Siegel, Herbert:
Hydrographisch-chemische Zustandseinschätzung der Ostsee 2007
Pohl, Christa; Hennings, Ursula:
Die Schwermetall-Situation in der Ostsee im Jahre 2007

73 (2008) Telesh, Irena; Postel, Lutz; Heerkloss, Reinhard; Mironova, Ekaterina; Skarlato, Sergey:
Zooplankton of the Open Baltic Sea: Atlas

74 (2008) Wasmund, Norbert; Pollehne, Falk; Postel, Lutz; Siegel, Herbert; Zettler, Michael L.:
Biologische Zustandseinschätzung der Ostsee im Jahre 2007

75 (2009) Hagen, Eberhard; Plüschke, Günter:
Daily Current Series in the Deep Eastern Gotland Basin (1993 – 2008)

76 (2009) Telesh, Irena; Postel, Lutz; Heerkloss, Reinhard; Mironova, Ekaterina; Skarlato, Sergey:
Zooplankton of the Open Baltic Sea: Extended Atlas

77 (2009) Nausch, Günther; Feistel, Rainer; Umlauf, Lars; Nagel, Klaus; Siegel, Herbert:
Hydrographisch-chemische Zustandseinschätzung der Ostsee 2008
Pohl, Christa; Hennings, Ursula; Leipe, Thomas:
Die Schwermetall-Situation in der Ostsee im Jahre 2008

78 (2009) Wasmund, Norbert; Pollehne, Falk; Postel, Lutz; Siegel, Herbert; Zettler, Michael L.:
Biologische Zustandseinschätzung der Ostsee im Jahre 2008

79 (2009) Wasmund, Norbert; Postel, Lutz; Zettler, Michael L.:
Biologische Bedingungen in der deutschen ausschließlichen Wirtschaftszone der Nordsee im Jahre 2008

80 (2010) Nausch, Günther; Feistel, Rainer; Umlauf, Lars; Nagel, Klaus; Siegel, Herbert:
Hydrographisch-chemische Zustandseinschätzung der Ostsee 2009
Pohl, Christa; Hennings, Ursula; Leipe, Thomas:
Die Schwermetall-Situation in der Ostsee im Jahre 2009

81 (2010) Wasmund, Norbert; Pollehne, Falk; Postel, Lutz; Siegel, Herbert; Zettler, Michael L.:
Biologische Zustandseinschätzung der Ostsee im Jahre 2009

82 (2010) Wasmund, Norbert; Postel, Lutz; Zettler, Michael L.:
Biologische Bedingungen in der deutschen ausschließlichen Wirtschaftszone der Nordsee im Jahre 2009

83 (2010) Matthäus, Wolfgang:
Germany and the investigation of the Baltic Sea hydrography during the 19th and early 20th century
Matthäus, Wolfgang:
Publications on the history of the marine research in Warnemünde/Germany

84 (2011) Nausch, Günther; Feistel, Rainer; Umlauf, Lars; Mohrholz, Volker; Siegel, Herbert:
Hydrographisch-chemische Zustandseinschätzung der Ostsee 2010

85 (2011) Wasmund, Norbert; Pollehne, Falk; Postel, Lutz; Siegel, Herbert; Zettler, Michael L.:
Biologische Zustandseinschätzung der Ostsee im Jahre 2010
Wasmund, Norbert; Postel, Lutz; Zettler, Michael L.:
Biologische Bedingungen in der deutschen ausschließlichen Wirtschaftszone der Nordsee im Jahre 2010

86 (2011) Nausch, Günther; Feistel, Rainer; Umlauf, Lars; Mohrholz, Volker; Nagel, Klaus; Siegel, Herbert:
Hydrographisch-chemische Zustandseinschätzung der Ostsee 2011

87 (2012) Schmidt, Martin; Eggert, Anja:
A regional 3D coupled ecosystem model of the Benguela upwelling system

Martin Schmidt, Anja Eggert

A regional 3D coupled ecosystem model of the Benguela upwelling system.

CONTENT

Leibniz-Institut für Ostseeforschung Warnemünde
IOW